Radar and Lightning Observations of Normal and Inverted Polarity Multicellular Storms from STEPS

SARAH A. TESSENDORF* AND STEVEN A. RUTLEDGE

Department of Atmospheric Science, Colorado State University, Fort Collins, Colorado

KYLE C. WIENS

Los Alamos National Laboratory, Los Alamos, New Mexico

(Manuscript received 11 July 2006, in final form 15 February 2007)

ABSTRACT

This study discusses radar and lightning observations of two multicellular storms observed during the Severe Thunderstorm Electrification and Precipitation Study. The Lightning Mapping Array data indicated that the charge structure of the 19 June 2000 storm was consistent with a normal polarity tripole, while the 22 June 2000 storm exhibited an overall *inverted* tripolar charge structure. The 19 June storm consisted of weaker convection and produced little to no hail and moderate total flash rates peaking between 80 and 120 min^{-1}. The cells in the 22 June 2000 storm were much more vigorous, exhibited strong, broad updrafts, and produced large quantities of hail, as well as extraordinary total flash rates as high as 500 min^{-1}. The National Lightning Detection Network (NLDN) indicated that the 19 June storm produced mostly negative cloud-to-ground (CG) lightning, while the 22 June storm produced predominantly positive CG lightning, peaking at 10 min^{-1} just after two cells merged. However, the Los Alamos Sferic Array indicated that many of the positive CG strokes reported by the NLDN in the 22 June storm were intracloud discharges known as narrow bipolar events. Negative CG lightning was also observed in the 22 June storm, but typically came to ground beneath an inverted dipole in the storm anvil.

1. Introduction

Reviews on thunderstorm electrification by Williams (1989, 2001) have noted that thunderstorms commonly have a charge structure consisting of a main midlevel negative charge region, with a positive charge above and usually a small positive charge region below. This charge structure is often referred to as the normal tripole. Recent evidence has suggested that other charge configurations occur within thunderstorms, however, including structures with more charge layers than the three in a normal tripole (Stolzenburg et al. 1998), as well as what are called "inverted" charge structures (Marshall et al. 1995; Krehbiel et al. 2000a; Rust and MacGorman 2002; Rust et al. 2005; Wiens et al. 2005). Inverted charge structures are the opposite of the normal charge structure configuration, with a main midlevel region of positive charge, and negative charge above and below. The inverted charge structure has also been suggested as a hypothesized charge structure that is conducive to producing positive cloud-to-ground (CG) lightning (Williams 2001).

An obvious research question that arises from these observations, and the focus of this study, is what possible dynamical and microphysical storm processes lead to inverted charge structures? The Severe Thunderstorm Electrification and Precipitation Study (STEPS; Lang et al. 2004) provided a unique dataset to evaluate this question for thunderstorms on the high plains. To date, the 29 June 2000 supercell from STEPS has been studied extensively (MacGorman et al. 2005; Tessendorf et al. 2005; Wiens et al. 2005; Kuhlman et al. 2006) and other case studies from STEPS have also emerged in the literature (Rust and MacGorman 2002; Rust et

* Current affiliation: NOAA/Earth System Research Laboratory, Boulder, Colorado.

Corresponding author address: Sarah A. Tessendorf, NOAA/Earth System Research Laboratory, DSRC R/CSD3, 325 Broadway, Boulder, CO 80305.
E-mail: sarah.tessendorf@noaa.gov

DOI: 10.1175/2007MWR1954.1

al. 2005; Tessendorf et al. 2007). This study addresses similar issues as those addressed in Tessendorf et al. (2005), Wiens et al. (2005), and Tessendorf et al. (2007) for supercell storms from STEPS; however, the present study is concerned with the charge structures of two *multicellular* storms from STEPS. One of these storms exhibited a normal polarity tripole charge structure, while the other exhibited inverted polarity charge structure. We will discuss the kinematic and microphysical differences between the two cases that might have led to their contrasting charge structures.

2. Data and methods

Instrumentation and observing systems operated during STEPS are outlined in detail in Lang et al. (2004). This study uses radar data from the triple-Doppler S-band radar network and lightning data from the National Lightning Detection Network (NLDN; Cummins et al. 1998), the three-dimensional Lightning Mapping Array (LMA; Rison et al. 1999) operated by the New Mexico Institute of Mining and Technology, and the Los Alamos Sferic Array (LASA; Smith et al. 2002) operated by Los Alamos National Laboratory. Observations from the LASA are discussed in the appendix.

a. Radar data and processing

The Colorado State University (CSU)–University of Chicago–Illinois State Water Survey (CHILL) polarimetric Doppler radar, the National Center for Atmospheric Research (NCAR) S-band polarimetric (S-Pol) Doppler radar, and the Goodland, Kansas, National Weather Service Weather Surveillance Radar-1988 Doppler (KGLD) composed the triple-Doppler radar network in which each radar was located approximately 60 km apart, forming a rough equilateral triangle configuration (Tessendorf et al. 2005, their Fig. 1).

Wind field syntheses were completed for 27 volume scans during the period 2318 UTC 19 June–0213 UTC 20 June 2000 and 11 volume scans during the period 2356 UTC 22 June–0108 UTC 23 June 2000. The radar data were interpolated onto a Cartesian grid using NCAR's Sorted Position Radar Interpolator (SPRINT; Mohr and Vaughn 1979) with a grid resolution of 0.5 km in both the horizontal and vertical directions. After the grid interpolation, the velocity data were globally unfolded by means of NCAR's Custom Editing and Display of Reduced Information in Cartesian Space software (CEDRIC; Mohr et al. 1986). The 19 June storm propagated through both the western S-Pol–KGLD dual-Doppler lobe and into the eastern S-Pol–CHILL dual-Doppler lobe, while the 22 June storm remained in the northern CHILL–KGLD dual-Doppler lobe for the entire analysis period. Thus, the three-dimensional wind fields were computed using the radial velocities from S-Pol and KGLD between 2318 and 0059 UTC[1] and from S-Pol and CHILL between 0106 and 0213 UTC for the 19 June storm. Radial velocities from CHILL and KGLD were used in the wind syntheses for all analysis times on 22 June. The speed and direction of storm movement were manually calculated for each case and used for the advection parameters in the synthesis. The vertical velocities in both cases were obtained using a variational integration of the continuity equation (O'Brien 1970).

The polarimetric data from CHILL and S-POL were edited, gridded, and used as input to a fuzzy-logic hydrometeor classification algorithm (FHC) adapted from Liu and Chandrasekar (2000) and Straka et al. (2000), using the same methodology as in Tessendorf et al. (2005). The FHC for 19 June used temperatures from the 0145 UTC 20 June National Severe Storms Laboratory (NSSL) Electric Field Meter (EFM) balloon sounding. The FHC for 22 June used the 0038 UTC 23 June NSSL EFM sounding. Additional analysis and interpretation of the electric field profile from this 22 June EFM sounding can be found in Rust et al. (2005). As in Tessendorf et al. (2005), hydrometeor echo volumes were also calculated for each radar scan time by multiplying the number of grid points that satisfied the FHC category of interest by the volume of a grid box (0.125 km^3). Calculations of total graupel echo volume included both low- and high-density graupel categories, and calculations of total hail echo volume included both small and large hail categories.

b. Lightning data and processing

The New Mexico Tech LMA measures the time and three-dimensional location of very high frequency radiation sources emitted by lightning discharges. For a given lightning flash, the LMA may locate hundreds to thousands of such sources resulting in detailed maps of the total lightning activity. To interpret charge structure using LMA data, we follow the methodology of Wiens et al. (2005). We analyzed individual flashes and identified charge regions using the bidirectional discharge model (Kasemir 1960; Mazur and Ruhnke 1993) as a guide. Because of the inherent nature of negative breakdown being more powerful than positive breakdown at LMA frequencies, the majority of sources in a

[1] Except at 0019 UTC, when S-Pol and CHILL were used in the absence of a KGLD volume scan near that time.

typical flash are interpreted as negative breakdown through a region of ambient positive charge. This majority of sources typically cluster over a shallow range of altitude. The remaining minority of sources typically cluster in a distinctly different range of altitudes that is interpreted to be a region of ambient negative charge. We thus bifurcate the LMA sources into two regions based on the height of the initial LMA source in each flash: all sources above the flash initiation height are interpreted to be in one polarity of charge, and the rest, below that height, are interpreted to be in the opposite polarity charge region. We infer which region is which based on the temporal evolution of the LMA sources, along with the overall number of sources above or below the flash initiation height. This method has its limitations, however, as we can only infer charge regions where LMA sources (from lightning activity) are detected. Some sources that we label as negative charge regions could also be from negative breakdown in the form of recoil streamers through a path previously established by the less powerful positive breakdown. Furthermore, it is probably not correct to assign a charge to LMA sources near the ground since they really just illustrate the discharge path on its way to the ground. Nonetheless, in the cases of LMA sources near the ground, selecting the height below which LMA sources are no longer in regions of ambient charge is quite arbitrary, therefore we have not corrected for this and all charge-coded LMA sources are based solely on the results of the bifurcation method described above.

To determine total (intracloud plus CG) flash rates from the LMA data, we used an algorithm developed at New Mexico Tech (Thomas et al. 2003) that sorts groups of 10 or more LMA sources into discrete flashes. The minimum source threshold for flash grouping is somewhat arbitrary, but based on sensitivity tests in Wiens et al. (2005), a 10-source threshold captures the trends in the flash rate without being contaminated by singletons (single-source flashes that could lead to unrealistic flash rates). However, CG flashes cannot be confidently identified using only LMA data because the resolution of leaders to ground, as well as the vertical location accuracy for sources near the ground, is poor (Thomas et al. 2004). Therefore, we rely on the NLDN data for CG detection, though there are also limitations of the NLDN dataset that must be considered. For example, as described in the appendix, observations by the LASA indicate that many of the positive polarity CG flashes identified by the NLDN in the storm on 22–23 June may have been intracloud discharges known as narrow bipolar events (NBEs; Le Vine 1980; Willet et al. 1989; Smith et al. 1999, 2002).

3. Environmental conditions and case overviews

a. 19 June 2000

On 19 June 2000 a dryline had set up along the Colorado–Kansas border by 1000 UTC with surface dewpoints of 10°–15°C to the east of the dryline, and near 7°C to the west of the line (not shown). A 500-hPa trough was situated over Utah, giving way to mid-to-upper-level southwesterly flow into the STEPS region. Surface temperatures were near 30°C, but because of a very dry boundary layer the CAPE was minimal west of the dryline (Fig. 1). Surface winds were relatively weak and mostly southerly ahead of the dryline, and westerly rearward of the dryline. A ridge in surface equivalent potential temperature was situated in north-central Kansas and into south-central Nebraska, farther east of the STEPS domain (not shown).

By 2200 UTC 19 June 2000, a multicellular storm system developed near Colorado Springs, Colorado, and was traveling to the northeast toward the STEPS domain. A new cell developed southwest of the CSU–CHILL radar around 2300 UTC and was targeted by the STEPS operations center as a storm of interest (Fig. 2; hereafter storm 19A). By the beginning of the analysis period at 2318 UTC, this storm was already producing intracloud (IC) and mostly negative CG lightning (Fig. 2). The storm rapidly evolved while propagating to the northeast and was in its mature phase (see section 4a) by 0000 UTC. It passed over the CSU–CHILL radar near 0030 UTC and dissipated shortly thereafter. Near the time of storm 19A's dissipation, another group of cells was developing west of KGLD (hereafter storm 19B). These cells quickly began producing IC and mostly negative CG lightning, as they propagated to the northeast (Fig. 2). The cells of storm 19B eventually merged into an elongated storm by 0122 UTC, and between 0124 and 0154 UTC there were three reports[2] of severe winds greater than 25 m s^{-1} associated with this storm, the last of which was as high as 33 m s^{-1}. Storm 19B's peak in maximum updraft and graupel echo volume was observed around 0200 UTC (see Fig. 6). Shortly after this time, the storm quickly dissipated. The CG flash rates peaked right before dissipation.

b. 22 June 2000

A trough axis had set up in eastern Colorado by 1400 UTC 22 June 2000. Around 1900 UTC a line of convection was observed on radar situated along the

[2] Storm reports were retrieved from *Storm Data* online, maintained by the National Climatic Data Center.

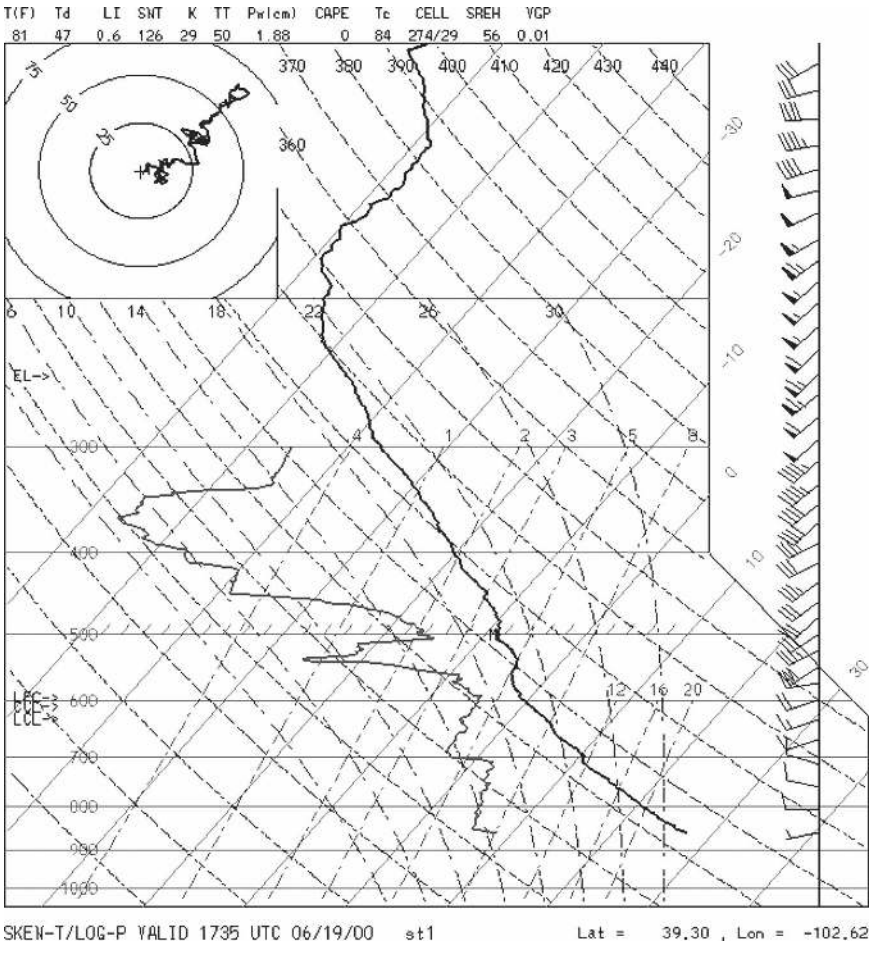

FIG. 1. M-GLASS thermodynamic sounding taken near Stratton, CO, at 1735 UTC 19 Jun 2000.

trough line and extending from northeastern Colorado into the Nebraska panhandle (not shown). A surface wind shift line was evident in the 2100 UTC surface observations, in conjunction with the trough axis, with southerly winds east of the line and northerly winds to the west of it. Surface temperatures in the STEPS domain were near 32°C, with surface dewpoint temperatures near 10°C (not shown). CAPE values, based on NCAR Mobile GPS/Loran Atmospheric Sounding System (M-GLASS) soundings taken in the area, were 500–600 J kg^{-1} (Fig. 3), which are modest for the region given the mean CAPE in June is between 800 and 1200 J kg^{-1} according to Grumm et al. (2005). This particular sounding in Fig. 3, which was one of the few soundings with complete data on this date, may not have fully represented the storm environment such that CAPE values nearest the storm could have been higher.

Near 2330 UTC 22 June 2000, a cell on the southern end of the line of convection entered the western portion of the STEPS radar network. This cell dissipated by 0000 UTC, but a new cell directly to its southeast developed by 2356 UTC (Fig. 4; hereafter cell 22A). No CG flashes of either polarity were observed in cell 22A. Another convective cell entered the radar domain at this time just north of the CSU–CHILL radar, propagating to the northeast (hereafter cell 22B). This cell had developed near 2300 UTC outside of the radar scanning area. A few positive and negative CG strikes were observed with cell 22B (Fig. 4). These two cells began to merge at 0009 UTC (hereafter the product of cells 22A and 22B will be referred to as cell 22AB). During the merger process the storm produced only negative CG flashes on its far eastern flank. Then about 10 min after the merger, a peak positive CG flash rate near 10 min^{-1} was observed by NLDN (Fig. 8); however, many of the NLDN-detected positive CG flashes during this peak may have in fact been NBEs (see the appendix). Just after the cell merger, the peak total flash rate was estimated by LMA to be near 500 min^{-1}. Between 0000 and 0030 UTC, hail up to 2.5 cm and sur-

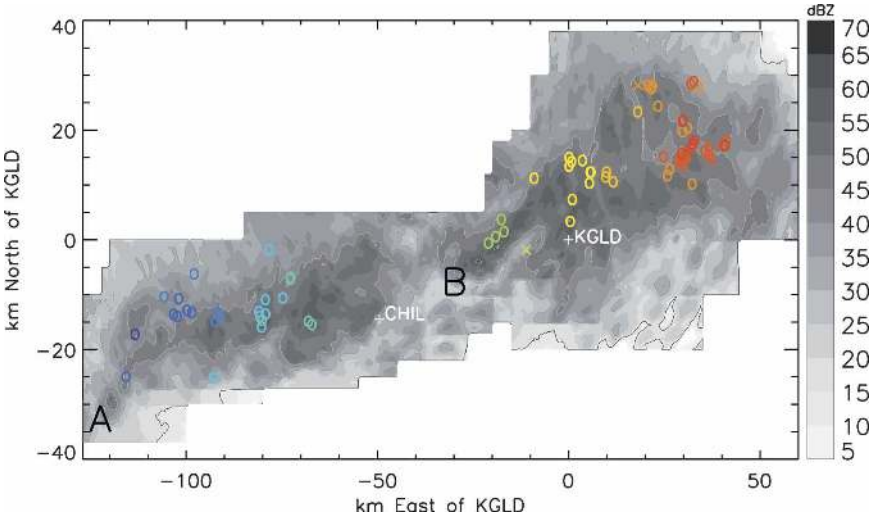

FIG. 2. Swath of composite reflectivity (grayscale) from the S-Pol radar accumulated over the analysis period 2318–0213 UTC 19 Jun 2000. NLDN CG lightning strikes are overlaid with an "O" for negative strikes and an "X" for positive strikes and color coded by time (progressing from blues to reds). The plus symbols represent the locations of the radars. Cells A and B have been labeled for reference.

face winds near 30 m s^{-1} were reported with this storm, according to *Storm Data* online. Beyond 0030 UTC, the storm continued to produce a few negative CG flashes, and the positive CG flash rate (according to the NLDN) was 1–3 min^{-1} until dissipation. Near the time of the merger, a new cell (hereafter cell 22C) developed to the south of cell 22AB. Beyond that time, cells 22AB and 22C continued to propagate to the east-northeast and evolved into a linear convective system (hereafter line 22ABC) beyond 0108 UTC. Another group of cells developed to the southeast of line 22ABC as it was dissipating near 0150 UTC. These new cells formed another linear convective system that propagated northeastward out of the STEPS radar network. The discussion from 22 June will focus on cells 22A, 22B, 22AB, and 22C.

4. Kinematic and microphysical observations

a. 19 June 2000

Using the maximum updraft velocity curve illustrated in Fig. 5, we define phases in each storm's life cycle on 19 June, which we will refer to later in the text. From the beginning of the analysis period at 2318 UTC until approximately 0000 UTC, storm 19A was in a developing phase, with the maximum updraft in this phase around 10 m s^{-1} (Fig. 5). After this point, the maximum updraft began to increase indicating the beginning of storm 19A's mature phase, with a peak updraft near 15 m s^{-1} at 0025 UTC (Fig. 5). After 0030 UTC, storm 19A entered its dissipating phase as the maximum updraft began to decline to around 6 m s^{-1} (Fig. 5). Storm 19A had essentially dissipated by 0052 UTC. At 0044 UTC, storm 19B began to develop and was targeted by the STEPS radar network. It remained in its developing phase until 0142 UTC when its maximum updraft quickly increased to near 10 m s^{-1} (Fig. 5). Storm 19B's mature phase (from approximately 0142 to 0208 UTC) was fairly short lived, and had a brief maximum updraft of 18 m s^{-1} just after 0200 UTC (Fig. 5). Storm 19B rapidly dissipated after 0208 UTC. The storm updraft volume exceeding 10 m s^{-1} (hereafter, UV10) was very small in these storms, composing no more than four percent of the total storm volume greater than 0 dBZ (which was on the order of 9×10^3 km^3; not shown), and peaking during the mature phases of each storm (Fig. 6).

Graupel was already identified by the FHC algorithm at the beginning of the analysis period in storm 19A, and graupel echo volume (hereafter, graupel EV) continually increased until 0025 UTC, during storm 19A's mature phase (Fig. 6). At its peak, graupel EV composed about 15% of the total storm volume (not shown). After this point, the total graupel EV dramatically declined. The dramatic decline is partially an effect of how the volumetric statistics were calculated. The two storms (19A and 19B) overlapped for about 20 min between 0044 and 0052 UTC. Thus, at 0044 UTC the total volume in which statistics are calculated increased to include the newly developing cells of 19B. At

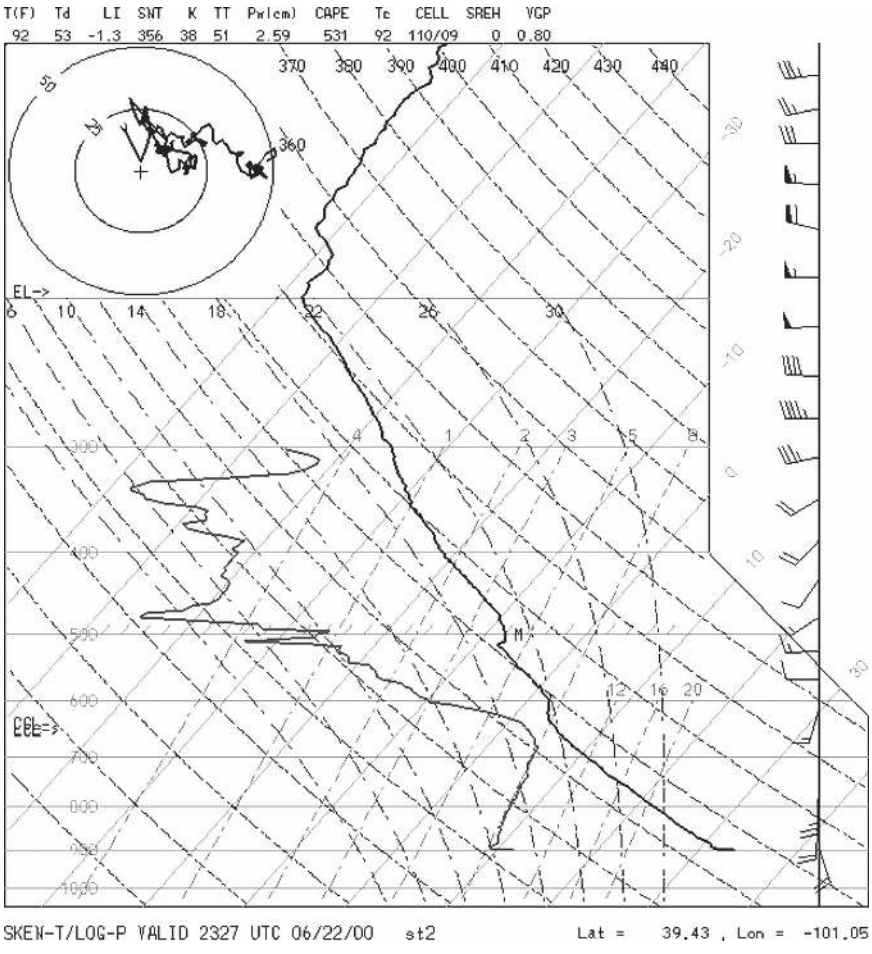

FIG. 3. M-GLASS sounding at 2327 UTC 22 Jun 2000 from near Goodland, KS.

0059 UTC, storm 19A had dissipated such that its volume was no longer included in the statistics calculations, resulting in a dramatic reduction in total graupel volume since the new cells were still quite small and did not yet contain much graupel. Nonetheless, storm 19B rapidly grew and attained volumetric statistics on par with storm 19A a short time later.

Most of the graupel EV was centered around 6 km (corresponding to a temperature near −10°C) until around 0030 UTC (Fig. 5).[3] After that time, during the dissipating phase of storm 19A, the center of the graupel echo lowered to near 5 km. In the developing phase of storm 19B, the graupel echo was centered around 4 km ($T \sim 0$°C) and the total graupel EV began to rapidly increase (Figs. 5–6). This rapid increase began ~30 min prior to the beginning of the mature phase of storm 19B (indicated by increased UV10 or maximum updraft), suggesting that at least part of the graupel EV detected within the boundaries of storm 19B at those times might have been from graupel grown in nearby convection and advected (or seeded) into the storm. This is suggested because the kinematics of storm 19B at that time were likely not sufficient to support the growth of hydrometeors into the observed quantities of graupel, and the convection on this day was multicellular making it both difficult to isolate the storm volume of storm 19B from nearby convection and more likely that hydrometeors could be advected from one storm to another. The total graupel EV reached its greatest peak at 0155 UTC during the mature phase of storm 19B, by which time the center of the graupel EV had also risen to 5 km.

The total hail echo volume (composed mostly of small hail) was negligible in this storm except for limited amounts detected near 7-km altitude at 0010–0020 UTC during storm 19A's mature phase, coincident with the local maximum in updraft speed of 14 m s^{-1} and

[3] All heights are in kilometers above mean sea level (MSL).

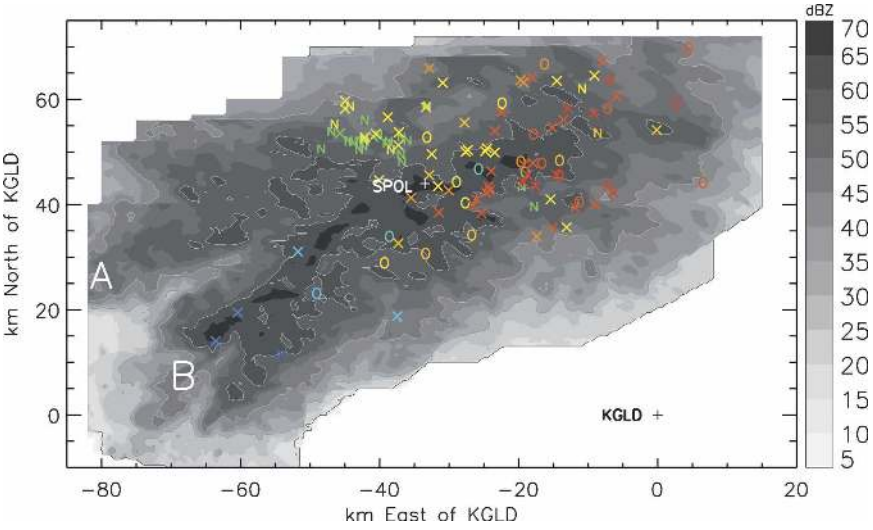

FIG. 4. Swath of composite reflectivity (grayscale) from the CSU–CHILL radar data accumulated over the analysis period 2356–0108 UTC 22 Jun 2000. NLDN CG lightning strikes are overlaid with an "O" for negative strikes and an "X" or "N" for positive strikes. Strikes labeled as "X" were detected by only the NLDN, while the strikes labeled as "N" were NLDN-detected positive strikes that were also detected by the LASA and had waveforms consistent with NBEs (see the appendix). All NLDN strikes are color coded by time (progressing from blues to reds). The plus symbols represent the locations of the radars. Cells A and B have been labeled for reference.

peak in UV10 (Figs. 5–6). For the most part, hail echo volume (hereafter, hail EV) was detected only near 3 km in the lowest portions of the storm, which is somewhat suspect because of possible brightband (surface wetting) effects (Fig. 5). As graupel particles fell through the melting level near 5 km and began to melt, the wet coating on the ice enhanced the radar reflectivity causing the FHC algorithm to misclassify these melting graupel particles as small hail. As the graupel completely melted on its descent to the surface, the specific differential phase (K_{dp}) values increased enough to nudge the FHC category to rain. This highlights some limitations of the FHC algorithm: it classifies hydrometeors based only on the current gridpoint's polarimetric values (i.e., it has no knowledge of what the hydrometeor types in the surrounding region or in the previous time step along a growth trajectory are) and there is no category for melting ice.

The total lightning flash rate (TFR) was around 10 min^{-1} at the beginning of the analysis period, and increased to near 60 min^{-1} by 0019 UTC during storm 19A's mature phase, coinciding with the time of peak graupel EV (Fig. 6). TFR declined for about 10 min around 2350 UTC, though a similar decline was not seen in the graupel EV trend (see Fig. 6). Both graupel EV and TFR decreased after 0019 UTC, and then the TFR began to rise again in storm 19B around 0052 UTC, when the total hail EV was also beginning to increase (Figs. 5–6). Graupel EV rapidly increased a short time later and peaked at the same time as the TFR and hail EV at 0122 UTC, but the graupel EV continued to rise beyond this time, while TFR and hail EV both declined until the end of the period. Consid-

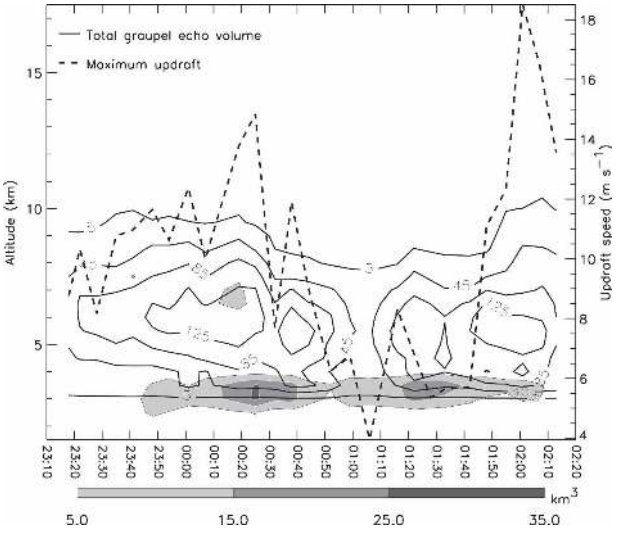

FIG. 5. Time–height contours of total graupel echo volume (solid black contours; beginning with 5 km^3 every 40 km^3) and total hail echo volume (grayscale contours), and maximum updraft time series (dashed black line; values on right axis) for 19 Jun 2000. For reference, storm A was observed from 2318 to 0052 UTC, and storm B from 0044 to 0213 UTC.

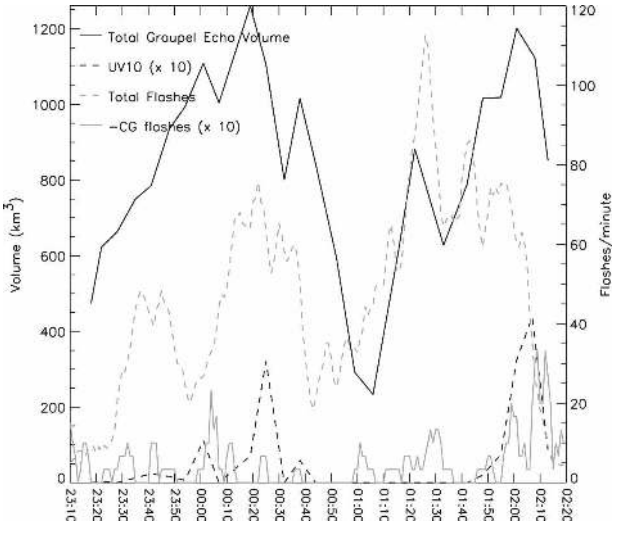

FIG. 6. Time series of the updraft volume greater than 10 m s^{-1} (dashed black line; ×10 to fit on left axis), the total graupel echo volume (solid black line; values on the left axis), the total lightning flash rate (using 10-source flash grouping; Thomas et al. 2003) from the LMA data (dashed gray line; values on the right axis), and the negative CG flash rate (solid gray line; ×10 to fit on the right axis) for 19 Jun 2000. For reference, storm A was observed from 2318 to 0052 UTC, and storm B from 0044 to 0213 UTC.

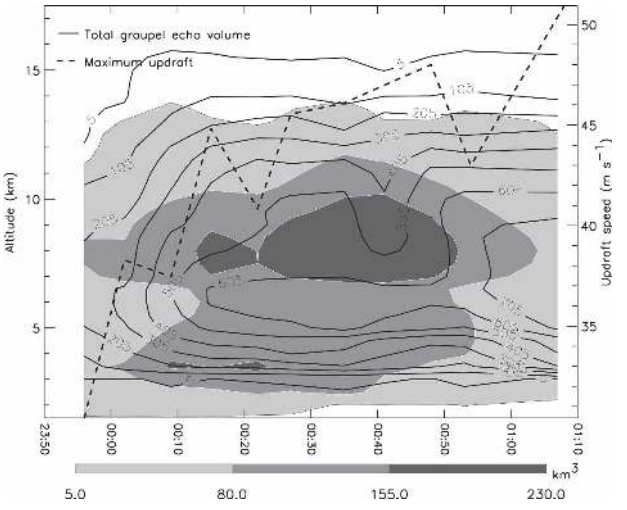

FIG. 7. Same as in Fig. 5, but for 22 Jun 2000 and the graupel echo volume contours are every 100 km^3. The statistics calculated in this time series include the volumes of both cells A and B for 2356–0002 UTC, and of cells AB and C for 0009–0108 UTC.

ering that this storm system was quite complex and rapidly evolving, it is difficult to rigorously interpret the relationships presented in these time series. Nonetheless, the observations indicate that, for the most part, TFR followed the behavior of graupel EV in storm 19A, while TFR seemed to follow the behavior of the hail EV in storm 19B. Keep in mind, however, that most of the total hail EV was in the small hail category, and much of that may have been melting graupel that was misclassified, rather than actual hail.

The CG flash rates from both storms were relatively low, but steady. Peak CG flash rates reached 4 min^{-1} during the dissipating stage of storm 19B (Fig. 6). There were, however, a few periods that were devoid of CG flashes: 0014–0021, 0040–0100, and near 0140 UTC (Fig. 6). These periods will be discussed in more detail in section 5.

b. 22 June 2000

The storms on 22 June 2000 were already nearing their mature phase when radar observations became available, and they remained in a mature phase for the duration of the analysis period. Therefore, we will not make reference to storm evolutionary phases in the following discussion. At the beginning of the analysis period at 2356 UTC, the maximum updraft velocity was already 30 m s^{-1} in both cells 22A and 22B (Fig. 7). By 0010 UTC when cells 22A and 22B were beginning to merge, the maximum updraft quickly increased to 45 m s^{-1} near the apex of the merger, and maintained these updraft strengths for almost an hour. By the end of the analysis period, the maximum updraft was near 50 m s^{-1} in cell 22C and 30 m s^{-1} in cell 22AB. These vertical velocities are higher than the theoretical limit predicted by the CAPE (Fig. 3). Though the dual-Doppler estimates of maximum vertical velocity are subject to several sources of uncertainty, it is possible that the storm environment had higher CAPE than that measured by the M-GLASS soundings. Additional observations of vertical velocity are not available to directly verify the dual-Doppler calculations; however, maximum updraft measurements along the flight track of the T-28 aircraft at an altitude of 6 km were near 30 m s^{-1} (A. Detwiler 2006, personal communication). The T-28 does not always penetrate the most severe updraft cores, however, and it typically flies at an altitude below where peak updrafts are observed, so the T-28 measurements can often be an underestimate of the true maximum vertical velocity.[4] Nonetheless, we also utilize UV10 as a measure kinematic intensity, and because it is based on a summation of points at which vertical velocity is greater than the 10 m s^{-1} threshold

[4] In the 29 Jun 2000 STEPS case (Tessendorf et al. 2005), Doppler-estimated peak updrafts were on the order of 50 m s^{-1}, while the peak updraft measured by the T-28 aircraft at 6 km was only near 37 m s^{-1} (A. Detwiler 2006, personal communication). On this day, a balloon did get into the updraft and confirmed maximum vertical velocities were near 50 m s^{-1} at about 8 km.

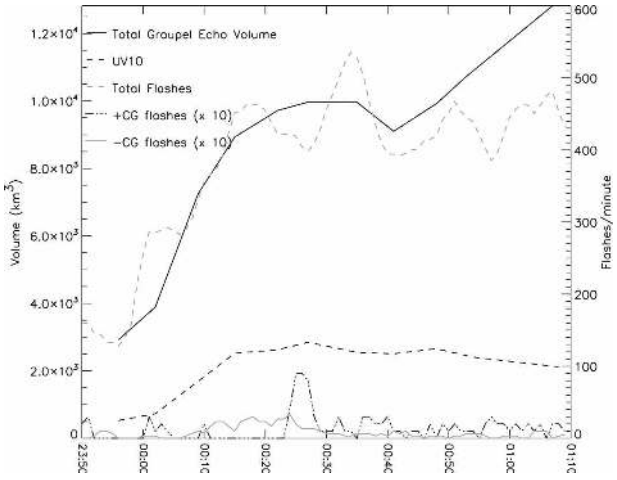

FIG. 8. Same as in Fig. 6, but for 22 Jun 2000, and including the NLDN positive CG flash rate (dash–dotted black line; ×10 to fit on the right axis). It is possible that the peak in positive CG flash rate was actually a peak in NBEs (see the appendix). The statistics include the same storm cell volumes as in Fig. 7.

rather than a single-point maximum, it is a more reliable measurement. In the 22 June storms, UV10 was on the order of 2×10^3 km^3 (Fig. 8), accounting for 6%–7% of the total storm volume (reflectivity > 0 dBZ) that was on the order of 3×10^4 km^3 (not shown).

The graupel EV maximum was centered around 6 km ($T \sim -10$°C) until 0050 UTC, when the EV broadened to between 5 and 9 km (Fig. 7). Graupel EV reached its maximum at the end of the analysis period, at the same time the peak maximum updraft was observed. The 5 km^3 contour of graupel EV reached heights of up to 16 km at times. The hail EV maximum was centered around 8–9 km and peaked between 0010 and 0050 UTC (Fig. 7).

Graupel was already indicated by the FHC algorithm at the beginning of the analysis period (Fig. 8), and throughout much of the time series, graupel EV represented about 30% of the total storm volume (not shown). As mentioned above, graupel EV peaked at the end of the analysis period and was coincident with the peak in maximum updraft, but not UV10, which peaked broadly between 0010 and 0050 UTC (Fig. 8). The aforementioned hail EV peak was coincident with this peak in UV10 (Figs. 7–8). As cell 22AB began to dissipate and lose UV10, much of the hail fell out. Thus, the total hail EV seems to relate more to UV10 than maximum updraft. This is consistent with studies by Nelson (1987) and Tessendorf et al. (2005) who showed that the area of strong updraft is also important for hail growth, in addition to the maximum updraft speed that typically governs the maximum hail size.

The TFR was already near 150 min^{-1} at the beginning of the analysis period, and rapidly increased to around 400 min^{-1} by 0010 UTC, coincident with the beginning of the cell merger process (Fig. 8). The TFR peak, which occurred just after 0030 UTC, within 10 min after the cell merger, was approximately 500 min^{-1}. TFR had a trend very similar to that of graupel EV (Fig. 8), which would be expected because collisions involving riming ice have been shown to be important in charging processes (Takahashi 1978; Saunders et al. 1991; Saunders and Peck 1998). The lower temporal resolution of the radar data (~7 min) to that of the LMA lightning data (1 min) likely contributes to the smoother appearance of the graupel EV curve relative to the TFR trend.

The positive CG flash rate (according to the NLDN data) was typically 1–3 min^{-1}, but increased to 10 min^{-1} just after cells 22A and 22B merged (Fig. 8). As discussed in the appendix, observations from the LASA indicate that the positive CG flashes identified by the NLDN during this spike were NBEs such that the apparent spike in positive CG flash activity was actually a spike in the NBE rate. Between 0011 and 0022 UTC, during the cell merger, the positive CG flash rate was zero, and only negative CG flashes were observed. The negative CG flash rate during this time was at its peak (3–4 min^{-1}; Fig. 8). The negative CG flash rate was typically 1–2 min^{-1} before and after this time period (Fig. 8). More details on the charge structure and the location of the negative CG flashes between 0011 and 0022 UTC will be discussed in section 5.

c. *Summary of kinematics and microphysics*

In summary, the 22 June case was much stronger than the 19 June case, as well as about 3 times larger than the 19 June case in terms of its total storm volume. The 22 June storm exhibited maximum updrafts as high as 50 m s^{-1}, greater than twice the strength of 19 June (see Figs. 5 and 7). The UV10 values on 22 June were two orders of magnitude larger than on 19 June for two reasons: 1) the 19 June storm rarely exhibited updraft speeds greater than 10 m s^{-1} and 2) updrafts were comparatively narrow in width compared with 22 June (see Figs. 6 and 8). The 22 June storm exhibited similar maximum updraft speeds and UV10 values on the same order of magnitude as the STEPS 29 June predominantly positive CG (PPCG) supercell (Tessendorf et al. 2005). The hail EV on 22 June had a strong maximum near 8–9 km indicating the presence of large precipitation ice in the mixed-phase region of the storm, whereas on 19 June the hail EV was negligible throughout the storm. The 19 June convection was also not as deep as that on 22 or 29 June (Tessendorf et al. 2005). The 5-km^3 contour of graupel EV typically was observed as

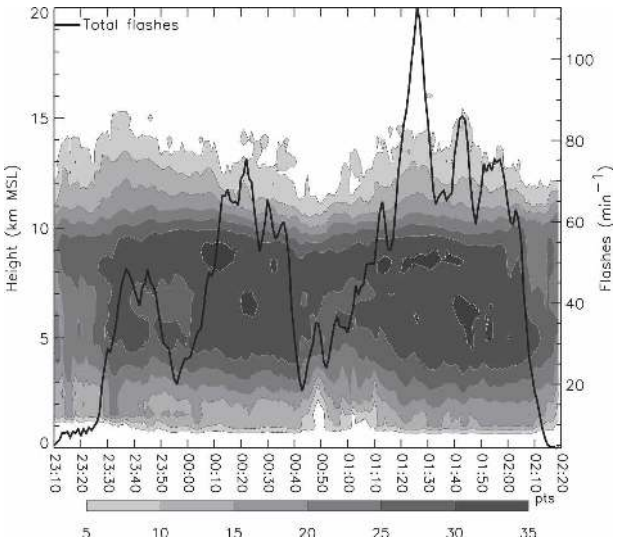

FIG. 9. Time–height contours of the total number of LMA sources (grayscale in logarithmic units) with the total flash rate time series overlaid in black for 19 Jun 2000.

high as 15 km in the two storms of 22 and 29 June, whereas it was never observed above 10 km on 19 June (Figs. 5 and 7).

The lack of hail on the 19 June storm can most likely be attributed to the lack of updraft of sufficient strength and size to support hail growth. Thermodynamic conditions may have prevented the 19 June storm from achieving stronger updrafts necessary for hail growth, because the CAPE west of the dryline (in the region where the 19 June storms formed) was near zero, compared with being near 500 J kg^{-1} on 22 June (see Figs. 1 and 3). Furthermore, the surface inflow on 22 June was southerly to southeasterly bringing in much more humid air, compared to the surface westerlies on 19 June.

5. Lightning and charge structure

a. 19 June 2000

The bulk of the LMA sources were distributed throughout the entire storm depth between 2 and 11 km, with local maxima near 9 and 5–6 km (Fig. 9). LMA source density alone cannot be used to infer charge structure, but it does highlight regions of likely positive charge (given that most LMA sources are most often associated with negative breakdown in regions of positive charge). This depiction of the charge structure is not robust, however, given that many of the LMA sources are in the inferred (from flash-by-flash analysis) negative charge layer near 7 km (Figs. 9–11). Thus, flash-by-flash analysis is required to better determine the true complexity of the storm's charge structure, in particular to identify that there was indeed an intervening negative charge layer near 7 km. Nonetheless, in the less electrically active phases of the time series when the total flash rate is lower, a dearth of LMA sources near 7 km is evident, coinciding with the height of the inferred negative charge region (Fig. 9).

In both storms 19A and 19B, IC flashes were most often observed by the LMA near the reflectivity core, initiating at heights of 8 and 5 km (Fig. 10). Those flashes initiating near 8 km typically showed initial upward propagation, with many more LMA sources above the initiation height than below (Fig. 10), as seen by the consistent high-density layer of LMA sources just above 8 km in Fig. 9. The IC flashes originating near 5 km typically showed initial downward propagation, with the majority of LMA sources below the initiation height (Fig. 10). This vertical distribution of the LMA sources (along with analysis of individual flashes) indicates a region of positive charge around 8–11 km, a main midlevel negative charge region that is the source of the CG flashes around 5–8 km, and a lower positive charge layer below 5 km. This pattern, illustrated in Fig. 11, is consistent with a "normal tripole" charge structure (Williams 1989).

Figure 11 displays the radar observations and charge structure during six flashes, two of which are illustrated in Fig. 10, near 0019 UTC in the mature phase of storm 19A. These flashes illustrate the general charge structure observed in both storms 19A and 19B. Horizontal cross sections of reflectivity and vertical velocity show that the storm was multicellular, with multiple reflectivity cores, and the low-level updraft was east (ahead) of the advancing storm (Fig. 11). The vertical reflectivity structure of the storm 19A (which is similar to that of storm 19B) is shown in Figs. 11c,d. The main updraft was east (ahead) of the storm and under an overhang in reflectivity. The charge structure in the overhang region (and also the main updraft) resembled a normal dipole with a main negative charge region centered around 7–8 km, and an upper positive charge region above that at 9 km (Fig. 11d). In the core of the storm, a normal polarity tripole structure can be seen, with the additional lower positive region below 7 km (Fig. 11d).

In the LMA data, negative CG lightning flashes usually initiated around 4–5 km and then propagated downward into what is inferred to be a lower positive charge region below the main negative region. The lower positive charge is illustrated in Figs. 10–11, even though these figures only include LMA sources from IC flashes. This also demonstrates that the lower positive charge was involved in IC flashes, as well as CG flashes. The presence of a lower positive charge region involved in the CG flashes supports the idea that a lower charge

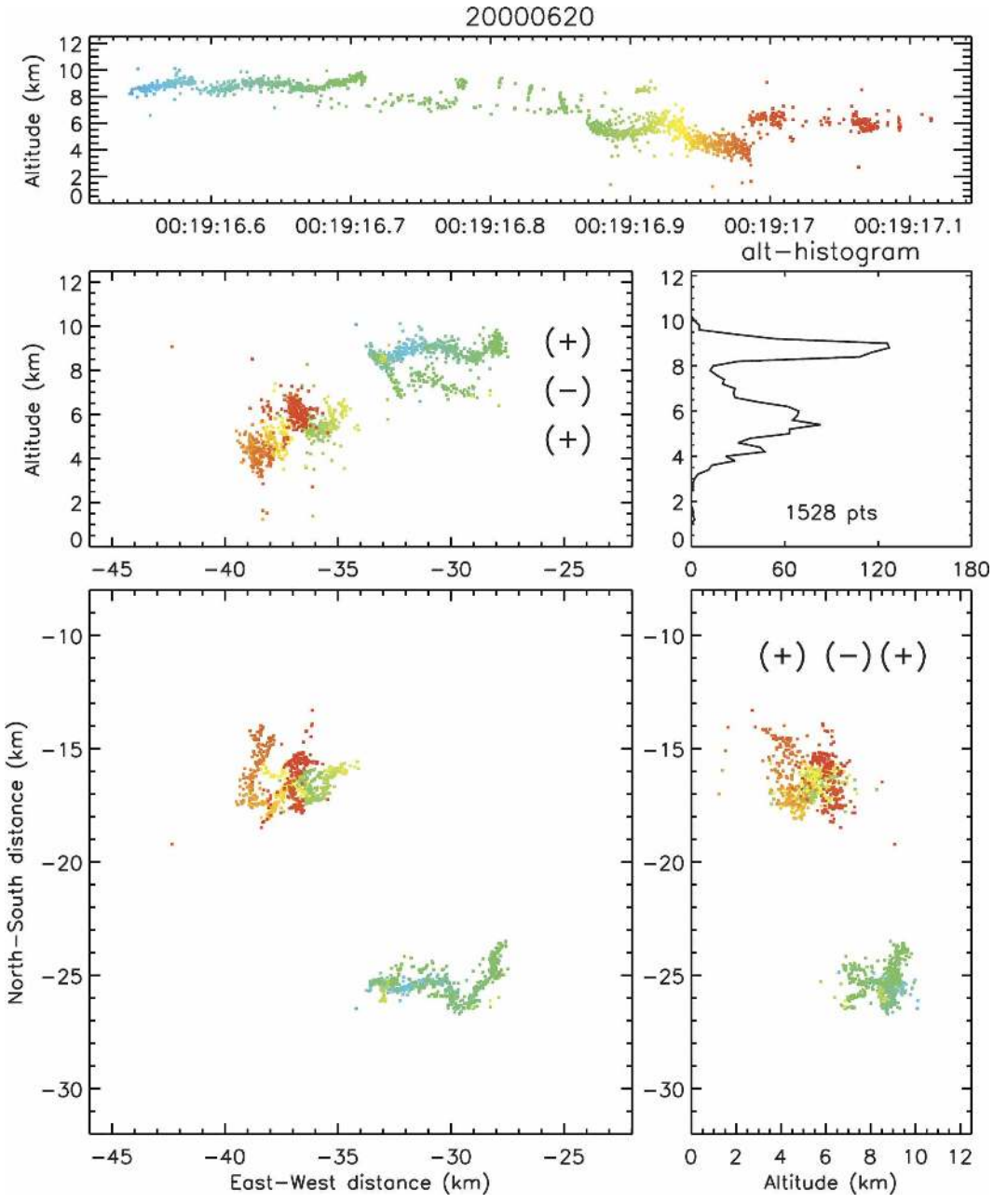

FIG. 10. Lightning mapping of a normal and inverted IC flash between 0019:16 and 0019:17 UTC 20 Jun 2000 color coded by time. The normal IC flash initiated near 8.5 km and progressed upward into inferred positive charge, while the inverted IC flash initiated near 6 km and progressed downward into inferred lower positive charge. The sparse sources below (above) the normal (inverted) IC flash initiation height are the inferred negative charge. This overall charge structure represents a normal tripole.

region, of opposite sign, may be needed to initiate CG lightning toward the ground (Williams 1989; Williams et al. 1989; Williams 2001; Mansell et al. 2002; Marshall and Stolzenburg 2002; Mansell et al. 2005; Wiens et al. 2005).

No CG flashes were observed in the mature phase of storm 19A between 0014 and 0021 UTC (see Fig. 6). Rather, there were numerous IC discharges between the lower positive and main negative regions (e.g., the second flash in Fig. 10). The LMA sources in the inferred lower positive charge region appeared vertically deeper and larger in area at this time as well. It is possible that, because many more IC discharges were detected between the main negative region and the

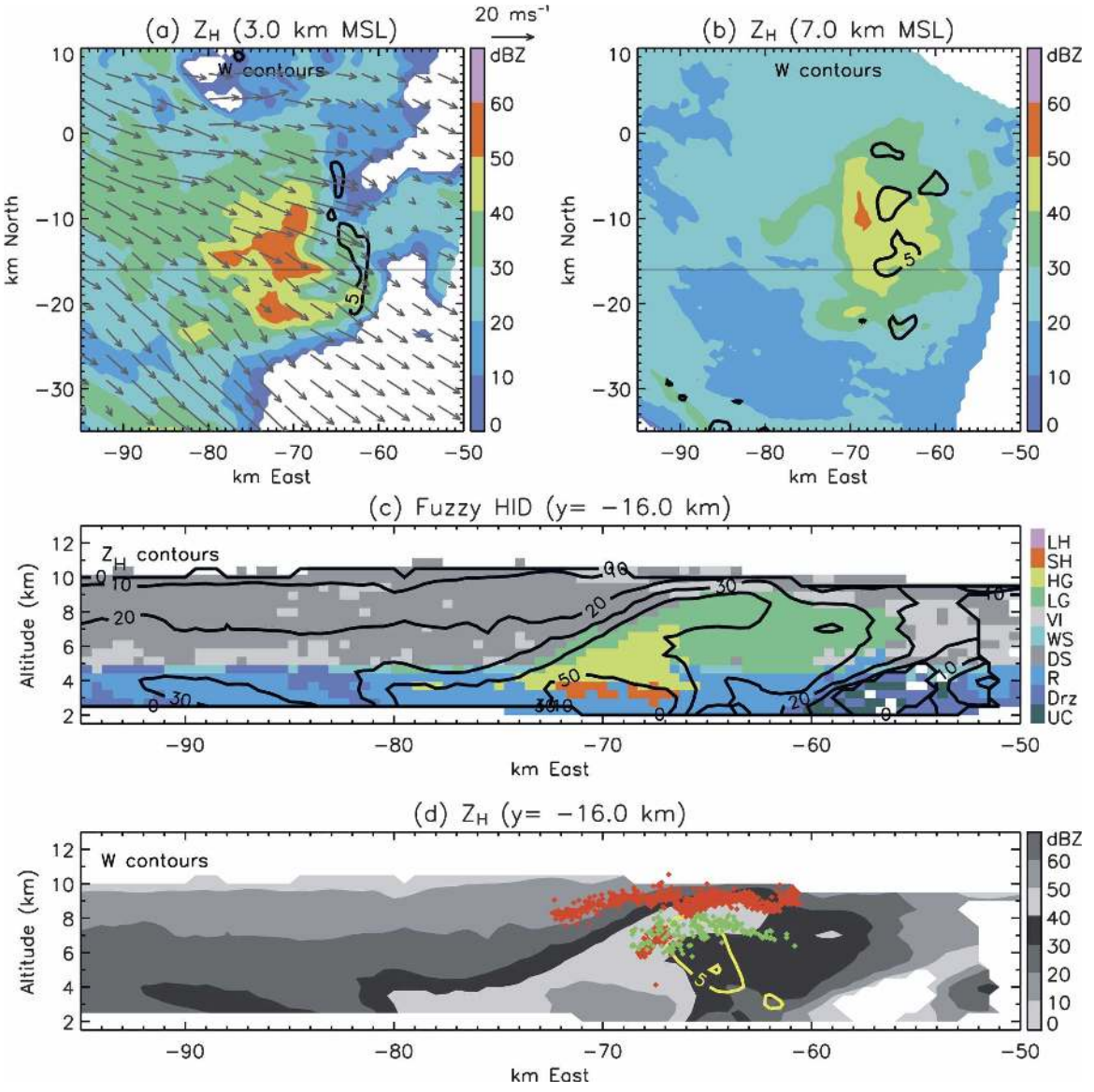

FIG. 11. S-Pol reflectivity at 0019 UTC 20 Jun 2000 at (a) $z = 3$ km MSL and (b) $z = 7$ km MSL, with updraft contours at 5 m s^{-1} overlaid in black, (c) FHC at $y = -16$ km with S-Pol reflectivity contours every 10 dBZ, beginning with 10 dBZ, overlaid in black, and (d) S-Pol reflectivity in grayscale with updraft contours at 5 m s^{-1} overlaid in yellow. Ground relative wind vectors are overlaid in gray in (a). LMA sources from six representative flashes within ±10 km of $y = -16$ km and between 0019:14 and 0019:17 are color coded as red (inferred negative breakdown in a positive charge region) and green (inferred positive breakdown in a negative charge region) and overlaid in (d). There were no NLDN strikes within the LMA time range for this figure. FHC categories are large hail (LH), small hail (SH), high-density graupel (HG), low-density graupel (LG), vertically oriented ice crystals (VI), wet snow (WS), dry snow (DS), rain (R), drizzle (Drz), and unclassified (UC).

lower (possibly deeper) positive region, IC discharges were more energetically favorable than negative CG flashes around that time (Marshall and Stolzenburg 2002). The LMA observations were similar to those in the mature phase of storm 19A during the absence of CG flashes near 0140 UTC in the mature phase of storm 19B. Between 0016 and 0022 UTC, there was also a lightning hole observed in the LMA data (not shown), which has been associated with stronger updrafts and bounded weak echo regions in horizontal cross sections of radar reflectivity (Krehbiel et al. 2000b; Wiens et al. 2005). A weak echo region and the core updraft were coincident with this lightning hole (not shown), and it was also during the period of peak maximum updraft (see Fig. 5).

For the period between 0040 and 0100 UTC, when

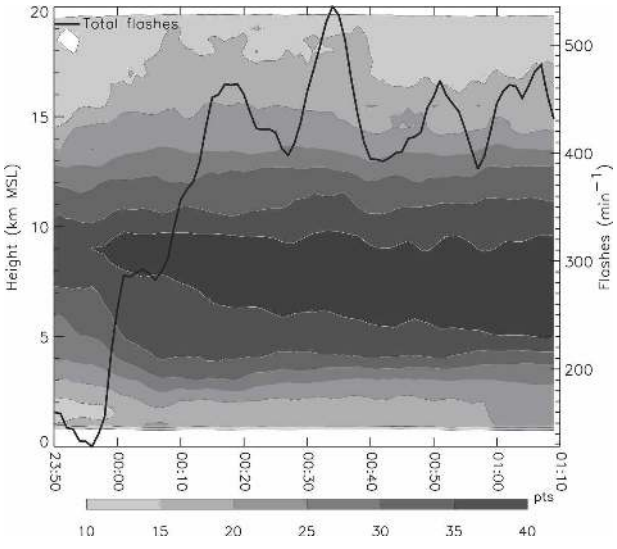

FIG. 12. Same as in Fig. 9, but for 22 Jun 2000.

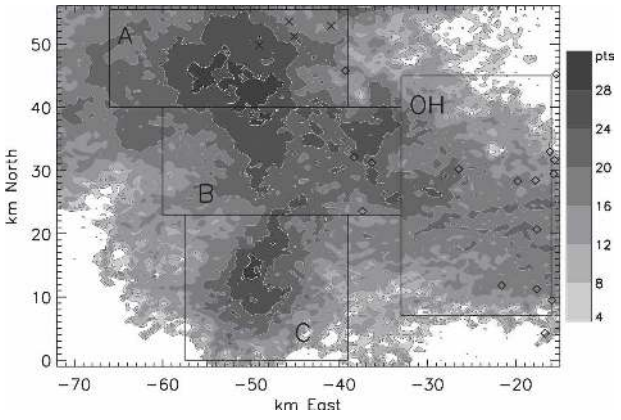

FIG. 13. Plan view of log of LMA source density (grayscale) between 0010 and 0020 23 Jun 2000. NLDN strikes during this 10-min period are overlaid in black as crosses for positive and diamonds for negative. Regions are labeled as cells A, B, C, and the overhang and anvil region (OH) for reference to the discussion in the text. Cells A and B are merging during this time period.

there was no CG activity (Fig. 6), the lower positive region was much less evident and thus the storm exhibited more of a normal dipole structure (see Fig. 9). Again, this supports the notion that in order for there to be CG lightning, a lower charge region is needed.

b. 22 June 2000

On 22 June, as seen in Fig. 12, a maximum of LMA sources around 9 km was evident from the beginning of the analysis period. This generally corresponded to a relatively well-defined and persistent inferred positive charge layer near a height of 9 km during this time period. After 0010 UTC, near the time of the cell merger, this maximum in LMA sources deepened and was centered around 8 km (Fig. 12), corresponding to a temperature of approximately −20°C. Total flash rates at this point exceeded 400 min^{-1}.

As might be expected from the extraordinarily large flash rates on 22 June, the charge structure of this storm system was very complex, and discrete charge layers representative of the entire storm at any given time could not be readily inferred. However, we will attempt to interpret the general charge structure, especially during periods of interesting CG activity. This interpretation is aided by considering the charge structure of individual regions of the storm, in particular, the eastern flank (i.e., reflectivity overhang and anvil region), the northern and central portions (formerly cells 22A and 22B, respectively), and the southern portion (cell 22C) highlighted in Fig. 13. The charge structures of cell 22C and the eastern flank of this storm system exhibited much more discernible and persistent charge layers than those of cell 22AB.

1) EASTERN FLANK

The eastern flank of the 22 June storm, labeled in Fig. 13 as the region "OH," consisted of the storm anvil (i.e., low radar reflectivity at high altitudes, suggesting the presence of small ice downwind of the reflectivity core) and the reflectivity overhang (higher reflectivity above a weak echo region associated with the updraft core). It consistently exhibited an area of inferred positive charge between 7 and 10 km, with inferred negative charge above that at 10–12 km (Fig. 14d). The CG flashes in this region were of negative polarity, and during the period between 0011 and 0022 UTC when negative CG lightning was dominant for the entire storm, those negative CG flashes were primarily located in the far eastern flank of the storm, beneath this inverted dipole (Figs. 13–14). The negative CG flashes typically originated from 9 to 10 km, tapping the upper negative charge. Reflectivity in the anvil area was fairly low (less than 30 dBZ; Fig. 14d), and unfortunately the scan sector from CSU–CHILL did not include this portion of the storm, so hydrometeor identification was not possible. However, the core of the storm was mostly graupel echo with some small and large hail (Fig. 14c).

Figure 14 also shows the time when cells 22A and 22B had just begun to merge, and when cell 22C was originally detected south of the subsequent cell 22AB merger (near $x = -55$, $y = 10$). The low-level wind vectors clearly show a region of convergence along the apex of the cell merger, with westerly motion in cell 22A and southerly winds in cell 22B (Fig. 14a). The updrafts were also organizing along this convergence line, and a broad region of updraft greater than 10 m s^{-1} was evident at 7 km (Fig. 14b).

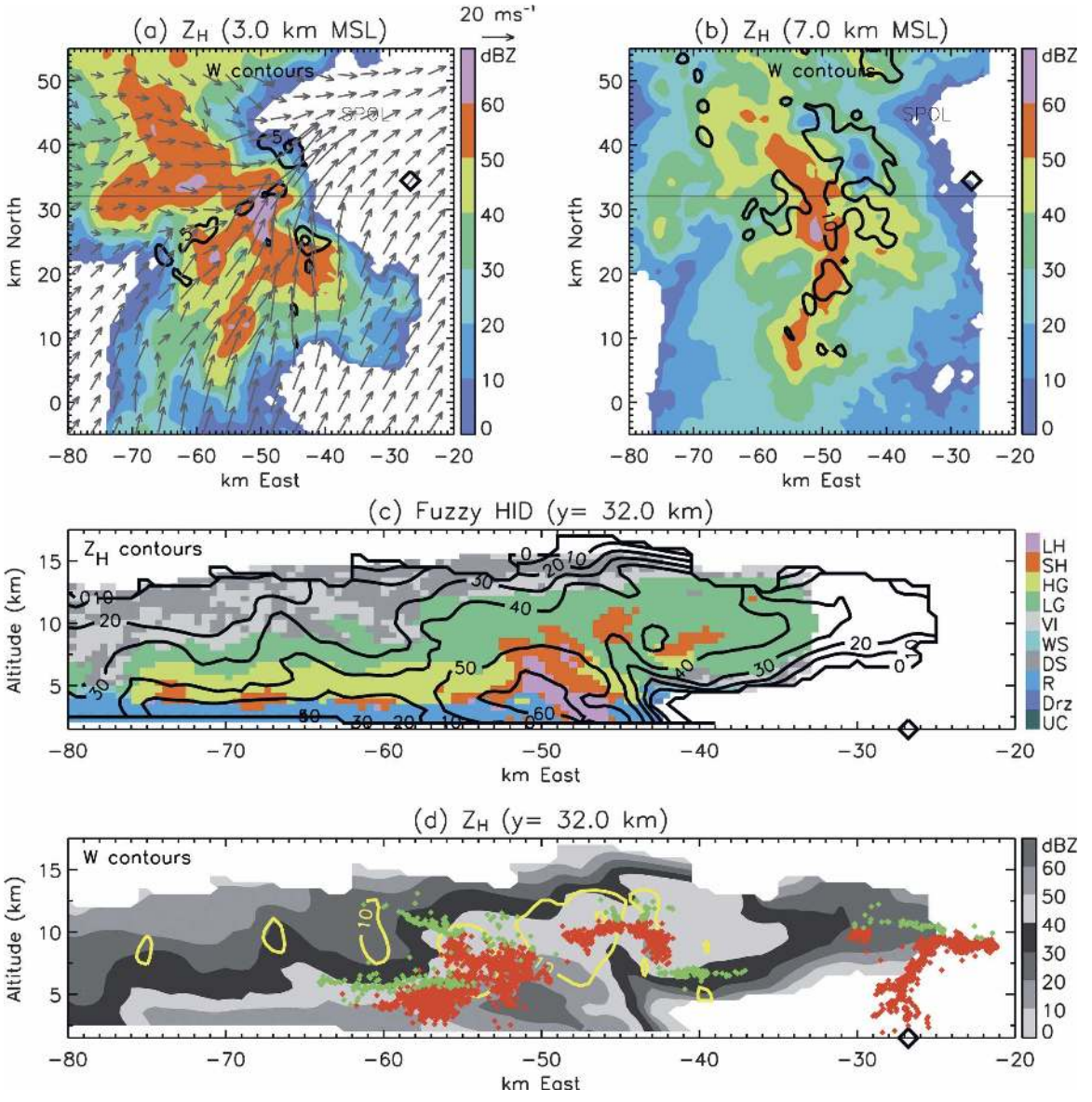

FIG. 14. KGLD reflectivity at 0009 UTC 23 Jun 2000 at (a) $z = 3$ km MSL with black updraft contours at 5 m s^{-1} and (b) $z = 7$ km MSL with a black updraft contours at 10 m s^{-1}, (c) FHC (from CSU–CHILL) at $y = 32$ km with KGLD reflectivity contours every 10 dBZ, beginning with 10 dBZ, overlaid in black, and (d) KGLD reflectivity at $y = 32$ km in grayscale with yellow updraft contours every 10 m s^{-1}, beginning with 10 m s^{-1}. Ground relative wind vectors are overlaid in gray in (a). LMA sources from approximately six flashes (including one negative CG) within ±10 km of $y = 32$ km and between 0013:32 and 0013:35 UTC are color coded as red (inferred negative breakdown in a positive charge region) and green (inferred positive breakdown in a negative charge region) and overlaid in (d). Negative polarity NLDN CG strikes within the LMA data time range are overlaid in (a)–(d) with a black diamond. FHC categories are the same as in Fig. 11.

2) NORTHERN PORTION (CELL 22A)

The first IC flash in cell 22A (the northern portion of the 22 June multicell; Fig. 13) was detected at 2356 UTC. It initiated near 10 km and propagated downward into an inferred region of positive charge between 7 and 9 km. Beyond this time, multiple charge layers were detected in cell 22A from the IC flashes, but there was no CG activity until after it merged with cell 22B at 0024 UTC. More specifically, inferred negative charge was present above 10 km, inferred positive charge resided between 8 and 10 km, another layer of inferred negative charge was observed between 6 and 8 km, and a second layer of positive charge resided between 4 and 6 km (as shown in the western portion of the vertical cross section in Fig. 15). A generalization of this charge

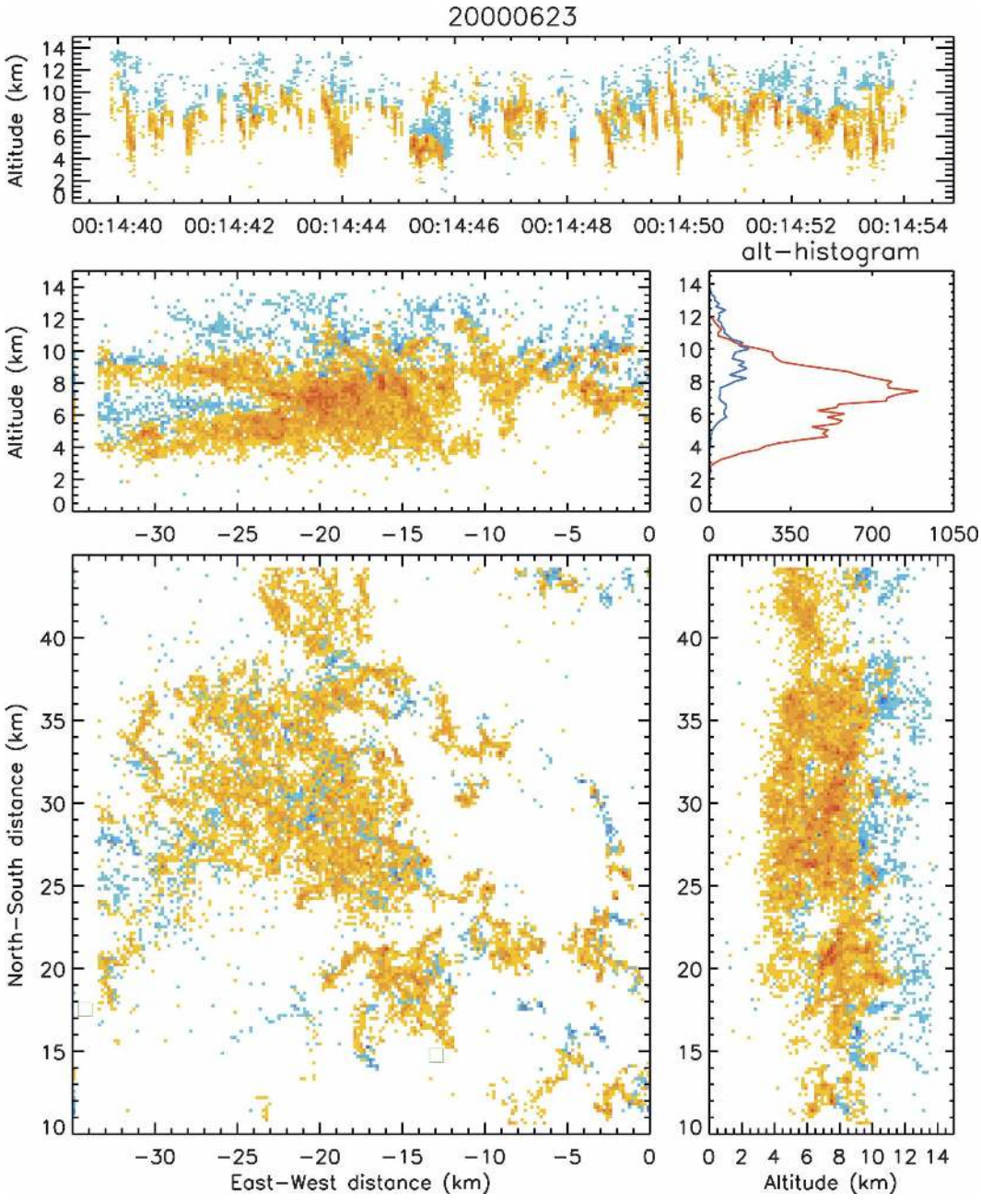

FIG. 15. Lightning mapping of several IC flashes between 0014:40 and 0014:54 UTC 23 Jun 2000. Sources are color coded by inferred charge density (warmer colors are greater density of sources in the inferred positive charge, while cooler colors are greater density of sources in the inferred negative charge). A quadrapole structure is evident on the western portion of this storm with four alternating charge layers, beginning with positive charge as the lowest layer near 4 km. On the eastern portion, there is a deep region of positive charge between 4 and 9 km, with negative charge above that.

structure from 2356 to 0020 UTC could be termed a quadrapole. Four-layer charge structures have been shown in other storms by Stolzenburg et al. (1998). By 0010 UTC (the beginning of the merger with cell 22B), the charge layers in the eastern portion of cell 22A became more complex and difficult to discern. However, positive charge was inferred over a considerable depth (between 4 and 9 km) in the eastern portion of the storm core, where the broad new updraft was developing and ingesting millimeter-sized drops as in-

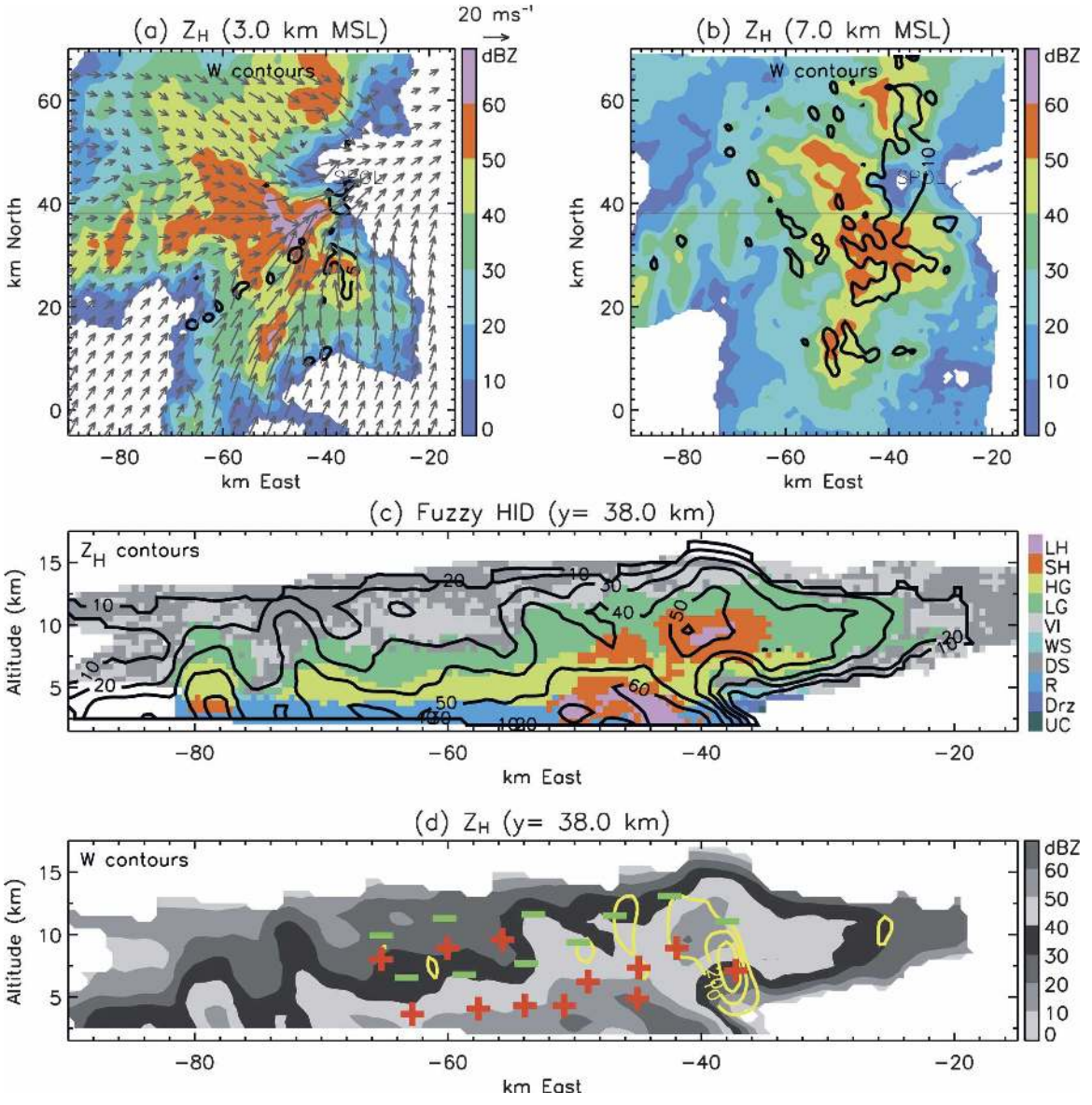

FIG. 16. Same as in Fig. 14, but at 0015 UTC 23 Jun 2000, and (b) 10 and 30 m s^{-1} contours are overlaid and (c), (d) y = 38 km. Red plus (green negative) symbols indicate the regions of inferred positive (negative) charge depicted in Fig. 15.

ferred from the elevated differential reflectivity (Figs. 15–17). A four-layer structure was still evident in the western portion of the cell during this time (Figs. 15 and 16d).

Figure 18 illustrates the radar structure at 0022 UTC, after cells 22A and 22B had merged into a large single cell, and cell 22C was at the southernmost tip (near $x = -50$, $y = 15$) of cell 22AB. The updraft was on the eastern (leading) flank, still in a region of low-level wind convergence. Very high reflectivities (>60 dBZ) were now evident aloft (at 7 km in Fig. 18b), indicating substantial precipitation ice aloft (also corroborated by FHC). A reflectivity overhang was still apparent, surrounding the main updraft (greater than 25 m s^{-1}), and the charge structure of the cell at this time was consistent with an inverted tripole (Fig. 18d).

3) CENTRAL PORTION (CELL 22B)

Cell 22B developed prior to the analysis period, near 2300 UTC, outside of the radar coverage area. The LMA data between 2300 UTC and approximately 2320 UTC indicate that this storm had a normal charge structure with upper positive charge inferred near 10 km, negative charge near 7–8 km, and lower positive charge

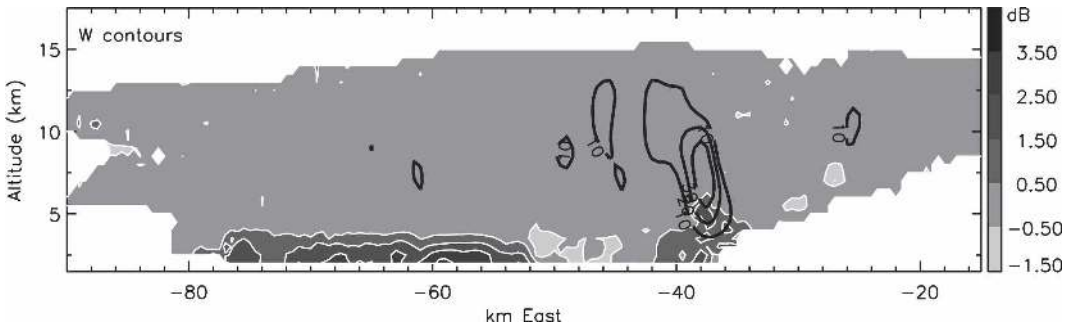

FIG. 17. Vertical cross section at $y = 38$ km (same as in Fig. 16) of differential reflectivity (Z_{dr}; gray shaded contours) at 0015 UTC 23 Jun 2000, with black updraft contours every 10 m s^{-1}, beginning with 10 m s^{-1}.

near 5–6 km (not shown). Soon after 2320 UTC, an extreme upper negative charge layer was inferred near 11 km, resulting in a quadrapole-like charge structure, similar to that observed in the early stages of cell 22A. During this time, the charge layers of the original normal tripole had also lowered by about 1 km, such that positive charge was situated near 9 km (below the extreme upper negative charge at 11 km), negative charge was inferred near 7 km, and the lower positive charge was at 4–5 km (not shown). Around 2340 UTC, the positive charge layer around 9 km deepened, and the lower positive charge layer disappeared, such that an inverted tripole charge structure remained. This is the charge structure observed in cell 22B when it entered the radar scanning area, at the beginning of the analysis period.

The central portion of the storm system (the area which was formerly cell 22B; Fig. 13) had a general inverted charge structure (see Fig. 14d). The upper negative charge was inferred between 9 and 12 km, with a region of main positive charge between 6 and 9 km, and lower negative charge in the core of the storm from 4 to 6 km. These charge layers tended to slope downward in height away from the updraft into the weaker precipitation (Fig. 14). Few CG flashes were detected within this portion of the storm, but those that were observed (in the first 20 min of the analysis period) were of positive polarity according to the NLDN (see the appendix). By 0015 UTC, shortly after cell 22B merged into cell 22A, the charge layer configuration in the merged 22AB cell was more complex compared with those in the cells prior to the merger (Fig. 16). Assuming the TFR estimate is reliable at this point, it is not clear if the more complicated charge structure led to a twofold increase in TFR following the merger or if the increased TFR led to more complicated charge structures. Coleman et al. (2003) noted that charge deposition from lightning adds complexity to charge structures. Similarly, Rust et al. (2005) suggested that lightning-deposited charge could have been a cause for some of the observed field changes in the EFM sounding through this storm system because lightning flashes occurred near its flight track. Moreover, flash initiation heights (indicating the height between two opposite charge layers where the electric field is enhanced and bidirectional breakdown initiates) broadened after the merger, illustrating the complexity of the new charge structure and possibly suggesting that there were more charge layers present to initiate IC flashes postmerger (not shown). Because of the complexity of this charge structure, however, we cannot quantify the number of charge layers at this point. Nonetheless, on the large scale there seemed to be a much deeper positive charge region (from 5 to 10 km), yielding a general inverted charge structure.

4) SOUTHERN PORTION (CELL 22C)

Cell 22C developed by 0010 UTC south of cell 22B as it was beginning its merger with cell 22A. At 0038 UTC an EFM balloon was launched on the west side of this cell and its flight path remained on the west side of cells 22C and 22AB. The charge structure inferred from this sounding exhibited complex multiple charge layers: a lower negative charge near 4 km, a deeper midlevel positive charge layer between 5 and 8 km, an upper negative charge layer near 12 km, and another positive charge layer above that (Rust et al. 2005). Within the deep midlevel positive charge layer, two intervening negative charge layers were observed by the EFM sounding, which may have been artifacts of horizontal balloon tracking or charge deposition (Rust et al. 2005). Based on the LMA, cell 22C exhibited a fairly persistent inverted tripole charge structure from its development through the end of the analysis period. An upper negative charge was inferred between 10 and 12 km, the main positive charge between 6 and 10 km, and a lower negative charge between 4 and 6 km (not shown).

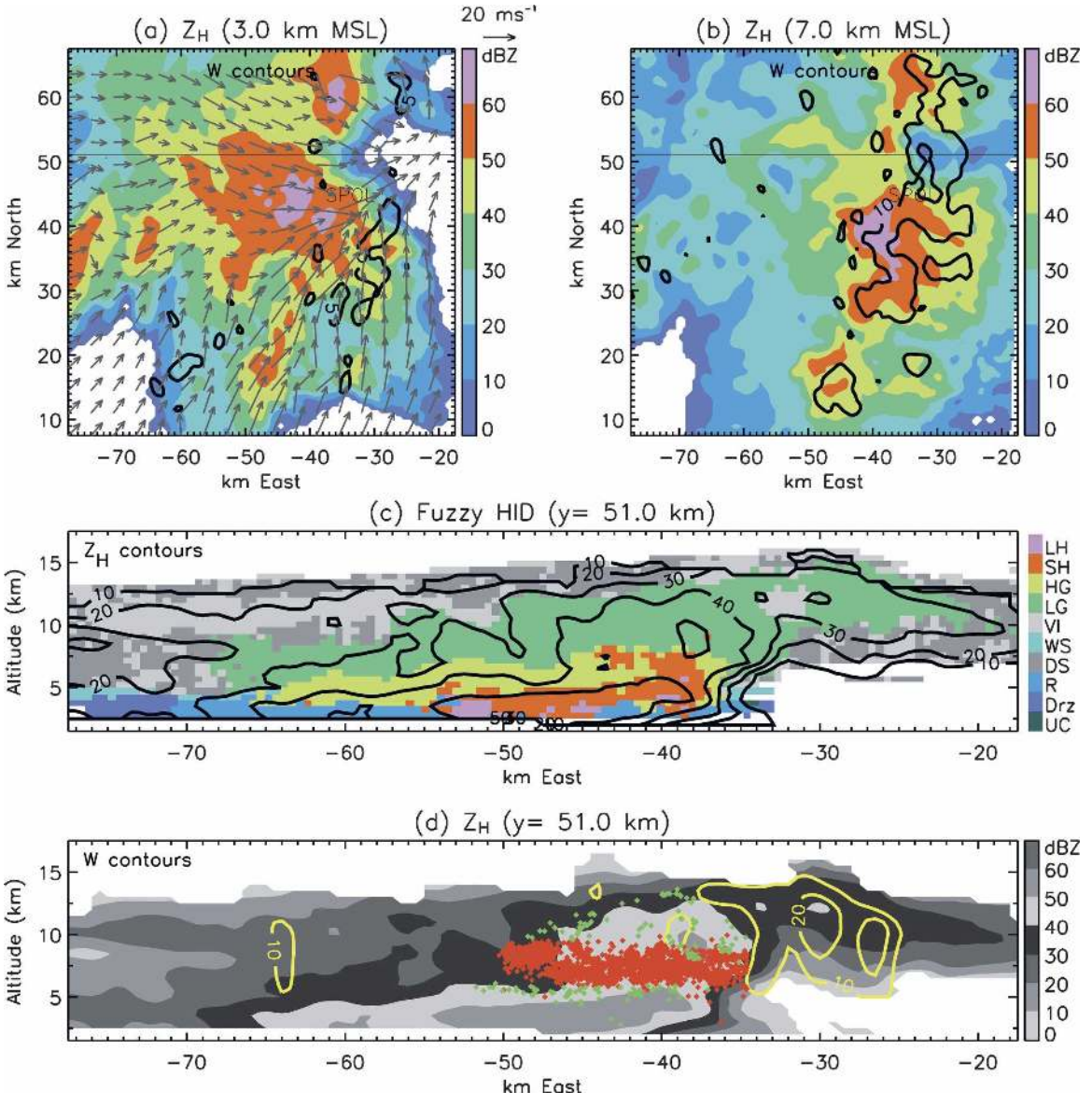

FIG. 18. Same as in Fig. 16, but at 0022 UTC 23 Jun 2000, and (c), (d) $y = 51$ km. (d) LMA sources from five IC flashes within ±10 km of $y = 51$ km and between 0025:03 and 0025:06 UTC are color coded as in Fig. 14 and overlaid.

These observations from the LMA are consistent with the inverted charge structure observed by the EFM sounding along the back (west) side of cell 22C, except that we did not detect an extreme upper positive charge layer with the LMA data.

c. *Summary of lightning and charge structure*

The 19 June storm consisted of weaker convection and produced little to no hail and average total flash rates on the order of 10 min^{-1}. The cells in the 22 June storm were more vigorous, exhibited strong, broad updrafts, and produced substantial quantities of hail, as well as extraordinarily large total flash rates exceeding 400 min^{-1}. Even when normalized by total storm volume, the TFR in 22 June was still 1.5 times as large as those in 19 June.

The LMA data indicate that the charge structure of the 19 June storms was consistent with a normal polarity tripole and, according to the NLDN data, CG lightning polarity was predominantly negative in both storms 19A and 19B (Fig. 19). The negative CG lightning in these storms typically originated near 5 km, between an inferred main negative region and a lower positive charge region. Furthermore, during the mature

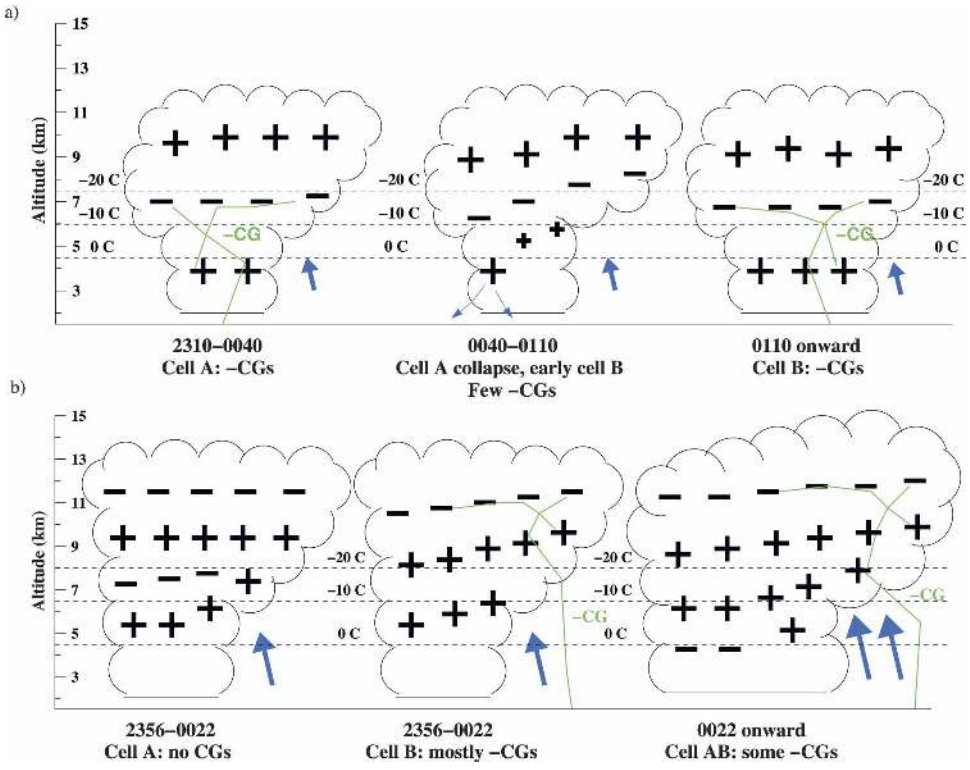

FIG. 19. Schematic drawings of the general charge structure evolution for the (a) 19 and (b) 22 Jun 2000 storms. Boldface blue arrows are a proxy for updraft, and thus their size and width scales accordingly. Thin blue arrows illustrate cell collapse and downdraft. Labels describe CG flash activity and dominant polarity for each time period. Green schematic flashes illustrate the charge layers involved in the negative CG flashes. The CG flashes are typically initiated between two layers of opposite charge around the heights where the schematic flash lines intersect. Positive CG flash activity has been omitted (see the appendix).

phases of 19A and 19B, brief lulls in the (negative) CG flash rate were observed, causing the IC:CG ratio to become infinite. Increased IC flashing between the lower positive and main negative charge regions occurred during these lulls in CG flashes suggesting that such IC discharges seemed to be preferred between the two lowest charge layers of the normal tripole. The LMA-inferred charge structure in the 22 June cells was dynamic and complex, but in general could be approximated by an inverted tripole with a deep midlevel positive charge region inferred during the analysis period (Fig. 19).

The negative CG lightning observed in the 22 June cells was typically under the anvil in a region with an *inverted* and elevated dipole charge structure. The negative CG flashes originated around 9 km between the upper negative and main positive charge layers of the inverted dipole. The CG flashes that come to ground below the main dipole, rather than below a tripole configuration, are still consistent with the concept that a lower opposite charge layer is needed for a CG flash, as long as the polarity of the CG flash corresponds to the upper layer in the dipole. For example, the bottom layer of the main dipole was of positive charge and was detected below negative charge, suggesting that a lower opposite charge layer was present in these *negative* CG flashes, just at a higher altitude than that of a typical negative CG. On another note, perhaps the reason that these flashes came to ground, instead of remaining IC flashes, was because the magnitude or depth of the lower positive charge in the anvil was small relative to that of the upper negative charge, such that the positive charge was quickly neutralized and the discharge continued to propagate to the ground (Marshall and Stolzenburg 2002). This latter condition may have been more common in the anvil than in the core of the storm, explaining the prevalence of negative CG flashes under the anvil.

The early charge structure in cells 22A and 22B consisted of four alternating layers of charge (with positive charge as the lowest layer), such that this could be termed a quadrapole (Fig. 19; similar to Stolzenburg et

al. 1998). This charge structure was also seen in the early developing phase of the 29 June supercell (Wiens et al. 2005). In the 19 June case, we observed the normal tripole, but we did not observe the fourth (upper negative) layer, perhaps because the storm was not as deep. The heights of the charge layers between the normal tripole of 19 June and the lowest three layers of the four-layer structures in 22 June were very similar. It appears that the four-layer charge structure of the 22 and 29 June cases evolved into a more general inverted tripole once they reached their respective intense phases. One might consider that the 22A and 22B storms charged normally (i.e., as a normal tripole) and then, by some means, evolved into an inverted tripolar structure. In cell 22C, however, an inverted tripole structure was observed from the beginning of its lightning activity.

6. Discussion and conclusions

Dramatic differences in kinematic intensity were observed between the 19 and 22 June storms. The 22 June inverted multicellular storm had similar maximum updraft speeds and UV10 as the 29 June inverted PPCG supercell (Tessendorf et al. 2005), while the 19 June normal polarity multicellular storm had UV10 values that were two orders of magnitude less and only half the maximum updrafts speeds as the two inverted storms. Lang and Rutledge (2002) showed that enhanced kinematic intensity was a distinguishing factor of PPCG storms compared with non-PPCG storms, and Williams et al. (2005) suggested that intense, broad updrafts provide conditions favorable for positive graupel charging, which could lead to inverted charge structures. Nonetheless, kinematic intensity is not likely to be the only factor leading to inverted charge structures and PPCG storms, since kinematically intense (severe) storms are observed in other regions of the United States and yet the CG lightning they produce is still mostly of negative polarity (Perez et al. 1997; Carey and Rutledge 2003). Cloud-base height (or warm cloud depth) and wind shear have been suggested as other factors that may influence the development of inverted charge structures and subsequent PPCG lightning (Williams et al. 2005; Wiens 2005), but further research is needed to better understand these relationships.

We should point out that both of the inverted storms did not have a clear inverted charge structure from the beginning (recall the four-layer structures of cell 22A and the 29 June supercell; Wiens et al. 2005), but after some event in the storm's evolution, perhaps surges in updraft speed and increases in UV10, the inverted charge structure became more apparent. Furthermore, the evolution of cell 22A into an inverted storm seems to be in conjunction with the development of the broad, strong updraft on the eastern flank of the cell. Recall that the four-layer, perhaps normal, charge structure was initially observed in cell 22A, and then as it merged with cell 22B a new broad updraft developed on the eastern flank, during which time a deep region of positive charge began to develop in the vicinity of that new updraft. The original four-layer charge structure was still evident, however, only in the western flank of the storm (Figs. 15 and 16). This may give further evidence in favor of the kinematic argument as at least part of the reason for inverted storms.

Hail production was also a distinguishing factor between the 19 and 22 June storms (as well as the 29 June supercell; Tessendorf et al. 2005), given that little to no hail was observed in the 19 June storm, while there were several reports of severe hail and large hail EV was observed on 22 June. It is possible that we commonly see hail in inverted storms because higher liquid water content (LWC) and strong kinematics are also conditions favorable for hail growth. At present, it is unclear whether the hail carries charge or is involved in charging that may invert the charge structure. Some studies suggest that hail is not an active participant in noninductive charging collisions, because of low number concentrations relative to graupel, and/or its tendency to grow in a wet or spongy configuration, which may cause ice crystals to stick, rather than rebound (Carey and Rutledge 1998; MacGorman et al. 2002; Kuhlman et al. 2006). Nonetheless, hail was present in the precipitation cores of the inverted storm discussed herein. Whether hail was actively involved in creating the inverted charge structure is beyond the scope of this paper, but warrants further study.

To the extent of our ability to detect the charge layers involved and/or present during the time of the negative CG flashes, a lower positive charge layer was present at all times when negative CG flashes were observed. (We were unable to determine the presence of a lower charge layer for positive CG flashes, and we are also suspicious of the NLDN positive CG reports in general, see the appendix). The use of the term "lower" here does not only refer to the lower positive charge layer in a normal tripole configuration, but also to the layer of positive charge that was located below the upper negative charge region of the inverted dipole involved in the 22 June negative CG flashes under the anvil. In general, we are referring to a layer of opposite charge being present below the charge layer that is discharged by the CG flashes. We also observed that IC flashes can occur between the middle and lower charge layers, and that the presence of a lower charge layer

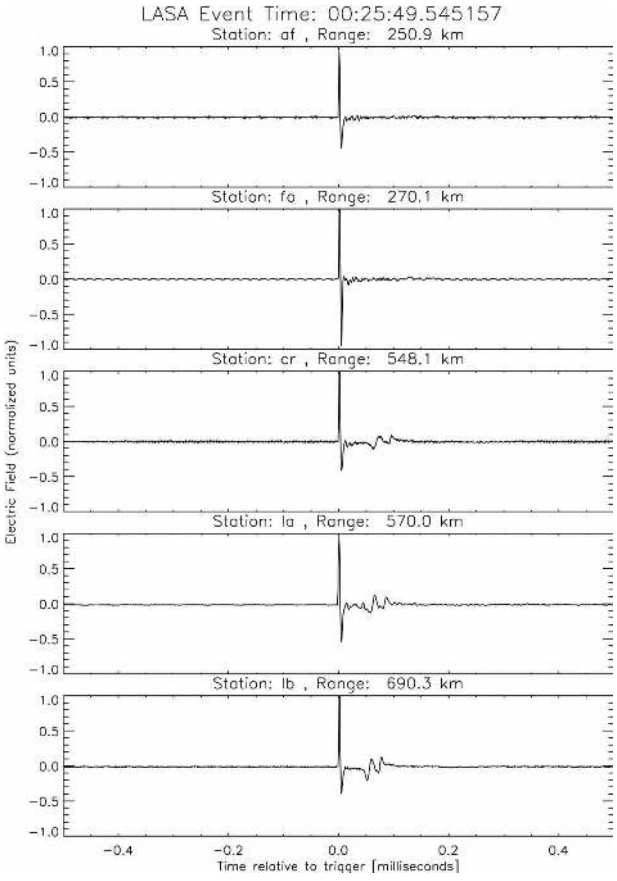

FIG. A1. Waveforms of a positive NBE detected by five LASA sensors. The event-to-station range is given above each waveform. The NLDN identified this discharge as a positive CG stroke with a peak current of 130 kA.

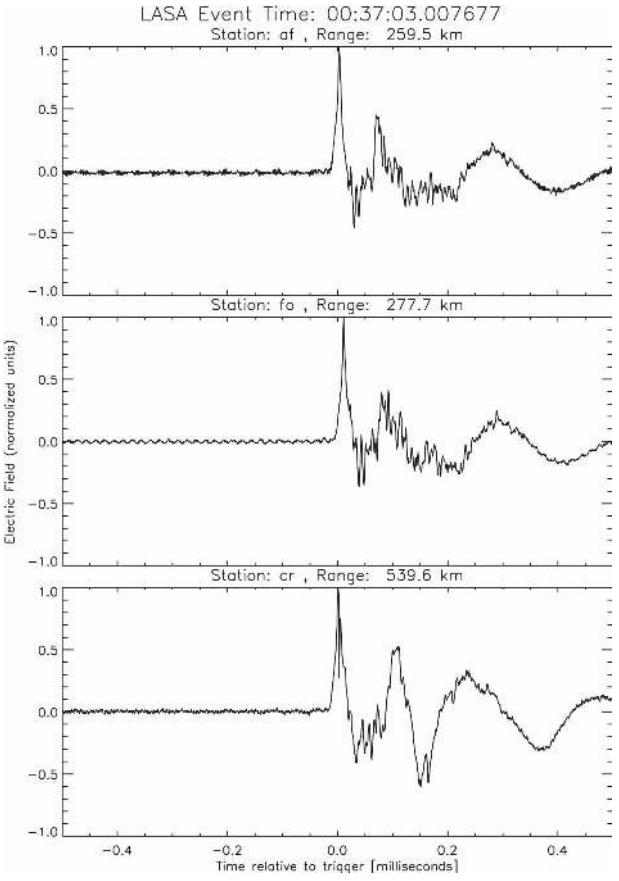

FIG. A2. Waveforms of a non-NBE detected by three LASA sensors. The event-to-station range is given above each waveform. The NLDN identified this discharge as a positive CG stroke with a peak current of 79 kA.

does not guarantee that CG flashes will occur. Nevertheless, when this lower opposite charge layer was not present, we did not observe CG flashes. Therefore, following the conclusions of Williams (1989), Williams et al. (1989), Mazur (2002), and Mansell et al. (2002, 2005), we conclude that the lower opposite charge layer may be necessary for a CG flash to come to ground. The lower charge layer of the tripole configuration, however, was typically not seen in the updraft core regions (i.e., under the reflectivity overhang), but rather in the region of the precipitation (reflectivity) core in the vertical cross sections.

An inverted *tripole* charge structure has now been documented in another storm from STEPS (in addition to the 29 June storm; Wiens et al. 2005), and enhanced kinematic intensity and hail production were distinguishing characteristics of this inverted storm, supporting the hypotheses of Lang and Rutledge (2002), Williams et al. (2005), and Wiens et al. (2005). Second, our observations reemphasize the importance of a lower positive charge layer in the production of negative CG flashes. Additional research is still needed to better identify and understand the specific storm processes that are involved in generating inverted charge structures and in developing the lower charge layer involved in CG flashes. Finally, an interesting future research question would be to study why the 22 June storm produced a burst of NBEs after the cell merger, and additional research is necessary to better understand NBE processes in relation to positive CG reports (see the appendix).

Acknowledgments. Support for the multiple-Doppler analysis was provided by L. Jay Miller (NCAR). Dr. Paul Krehbiel, Dr. William Rison, Dr. Ron Thomas, Dr. Tim Hamlin, Jeremiah Harlin, and Matt Briggs of New Mexico Tech provided the newly processed LMA data and XLMA software. Dr. Andrew Detwiler (South Dakota School of Mines) provided T-28 aircraft-based vertical wind observations for comparison

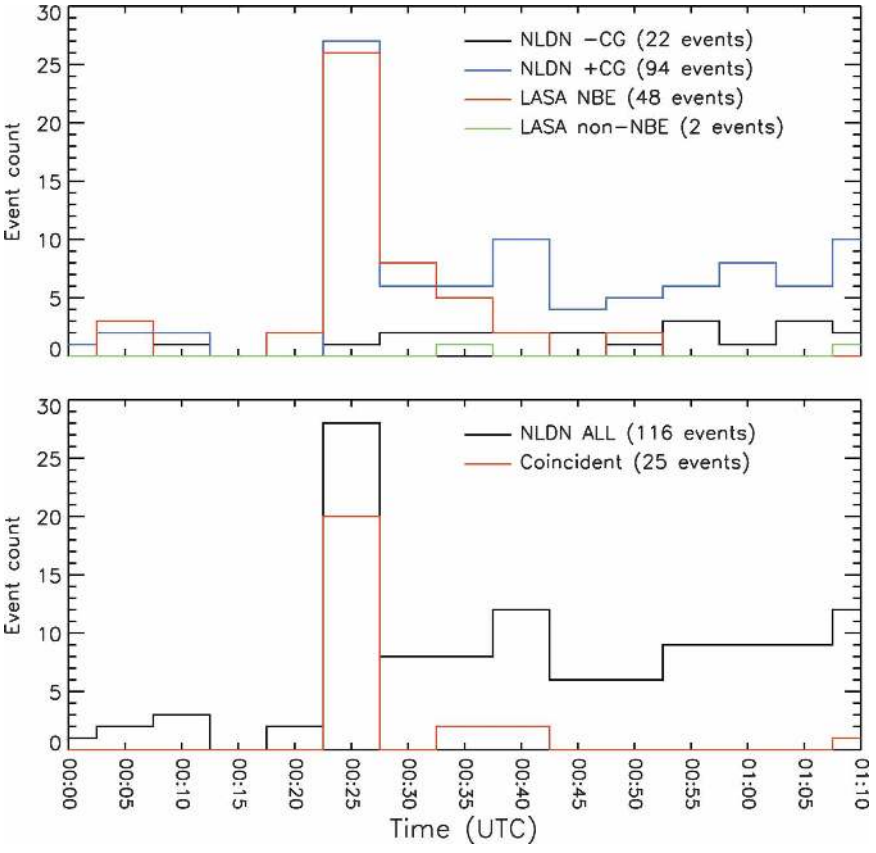

FIG. A3. Time series of NLDN and LASA event rates from 0000 to 0110 UTC 23 Jun 2000. (top) Event counts in 5-min bins of NLDN positive CG and negative CG events and of LASA NBEs and non-NBEs. (bottom) Event counts in 5-min bins of total NLDN events and NLDN events with coincident LASA events.

with the dual-Doppler analysis. We also acknowledge Drs. Rob Cifelli (CSU), Tim Lang (CSU), and Steve Nesbitt (University of Illinois at Urbana–Champaign) for their comments and internal review of this study. The CSU–CHILL radar is supported by the National Science Foundation (NSF) under Grant ATM-0118021 and Colorado State University. This research was supported by the NSF Physical Meteorology Program under Grant ATM-0309303.

APPENDIX

Suspect Positive CG Events in the 22 June 2000 storm

According to the NLDN, the 22 June 2000 storm produced PPCG lightning, with a pronounced peak in positive CG stroke rates during storm merger around 0025 UTC 23 June. However, independent measurements from LASA (Smith et al. 2002) indicate that many of the positive CG strokes identified by the NLDN were high-amplitude intracloud discharges known as NBEs. The purpose of this appendix is to compare the NLDN and LASA observations in order to evaluate whether these discharges were indeed positive cloud to ground.

a. NBEs

NBEs are a distinct class of IC discharges first detected by LeVine (1980) and Willet et al. (1989) and described in more detail by Smith et al. (1999). The term "NBE" typically refers to the discharge process itself, but the definition of a NBE is largely phenomenological. In terms of very-low-frequency–low-frequency electric-field-change waveforms measured by the LASA, NBEs are distinguished from ordinary CG and IC lightning discharges by their narrow ($\sim$10 μs) bipolar pulse widths, high signal-to-noise ratios, and their temporal isolation from other lightning-related electric field changes.

Figure A1 shows the waveforms of a NBE in the 22

June 2000 storm, as measured by five LASA sensors. For comparison, Fig. A2 shows the LASA waveforms of a positive CG return stroke in the same storm. The NLDN identified the discharges in both Figs. A1 and A2 as positive CG strokes. Note also in Fig. A1 that the NBE waveforms from the three more distant sensors have smaller-amplitude pulses that lag the initial large-amplitude pulse by 50–100 μs. These lagged pulses are due to reflections off the ionosphere and ground ionosphere. As described in Smith et al. (2004), these reflections are another hallmark of NBEs and can be used to determine NBE emission heights.

b. LASA–NLDN coincident events

As shown in the time series in Fig. A3, there were 116 NLDN events reported in the 22 June 2000 storm between 0000 and 0120 UTC 23 June. The LASA detected 50 events in the storm during this same time period. Most (94) of the NLDN events were identified as positive CG strokes, and 27 of these positive CG strokes occurred in a 5-min interval centered at 0025 UTC. All but two of the 50 LASA events were identified as NBEs, and 26 of these NBEs occurred in the 5-min interval centered on 0025 UTC. The task now is to determine the extent to which the LASA-identified NBEs were the same events as the NLDN-identified positive CG strokes.

To identify discharges that were detected by both the NLDN and LASA, the LASA events were searched to within 10 ms and 50 km of each of the 116 NLDN events detected within the storm under study. This resulted in 25 coincident events, which are summarized in Table A1. Though the time window used for searching for coincident events was 10 ms, the actual differences between NLDN and LASA event times were less than 1 ms in all cases. The NLDN reports give event times to only millisecond precision, whereas the LASA event times are reported to microsecond precision. The agreement between LASA and NLDN event times in Table A1 is thus as good as can be expected, and the mean time difference of 0.5 ms is consistent with the given precision of the NLDN event times. Note also that the NLDN versus LASA event locations agree to within a few kilometers (Table A1). Hence, to the extent that the given NLDN timing precision allows, the 25 events listed in Table A1 are truly coincident between the NLDN and LASA.

Of the 25 coincident events, 23 were identified as NBEs by the LASA. The other two were identified as positive CG strokes. Of the 23 coincident NBEs, 20 of them occurred during the 5-min interval centered at 0025 UTC. Hence, 20 of the 27 NLDN-identified positive CG strokes that occurred during this 5-min interval were identified as NBEs by LASA. LASA also identified six additional NBEs during this same time interval that were not coincident (within 10 ms) with NLDN-identified positive CG strokes.

TABLE A1. Information about the 25 LASA–NLDN coincident events on 23 Jun 2000.

NLDN time (UTC)	Time difference (LASA − NLDN) (ms)	Location diff (km)	NLDN peak current (kA)	LASA NBE?
0024:13.566	0.577	1.7	75.8	Yes
0024:43.167	0.794	0.9	90.0	Yes
0025:02.860	0.819	0.8	86.7	Yes
0025:14.702	0.505	1.6	120.7	Yes
0025:15.165	0.886	1.1	88.4	Yes
0025:23.719	0.145	1.4	85.4	Yes
0025:49.545	0.157	0.4	130.3	Yes
0025:51.959	0.665	1.4	88.8	Yes
0025:55.310	0.094	1.6	127.9	Yes
0025:55.721	0.550	0.9	80.3	Yes
0025:58.277	0.307	1.5	82.6	Yes
0026:10.655	0.741	1.5	76.3	Yes
0026:21.806	0.851	1.9	100.5	Yes
0026:26.067	0.820	2.1	97.7	Yes
0026:31.304	0.714	0.7	71.5	Yes
0026:39.794	0.024	1.5	101.8	Yes
0026:48.743	0.138	1.4	82.8	Yes
0027:01.313	0.520	1.3	88.9	Yes
0027:06.542	0.116	1.1	80.8	Yes
0027:09.842	0.294	1.8	90.7	Yes
0032:55.457	0.394	0.9	65.6	Yes
0037:03.007	0.677	3.4	79.4	No
0037:32.484	0.859	1.3	110.2	Yes
0041:31.163	0.069	0.5	81.4	Yes
0110:05.559	0.129	2.9	59.8	No
Mean	0.509	1.4	89.8	

To ensure that these events were indeed NBEs, we inspected all of their waveforms. Figure A1 shows an example. All of the waveforms for the LASA-identified NBEs very closely resemble those in Fig. A1 and show all the hallmarks of NBEs. We must conclude that the NLDN misclassified these 23 events.

c. Peak currents

As described in Cummins et al. (1998), the waveform acceptance criteria used by the NLDN are configured to accept (and thus report) only CG return strokes and to reject IC processes. However, increases in NLDN sensitivity and changes to NLDN waveform acceptance criteria led to NLDN detection and reporting of small-amplitude positive discharges that are likely not CG processes. Thus, Cummins et al. (1998) recommend that positive discharges with peak current less than 10 kA should be regarded as IC discharges. However, such thresholding on peak current would not have excluded

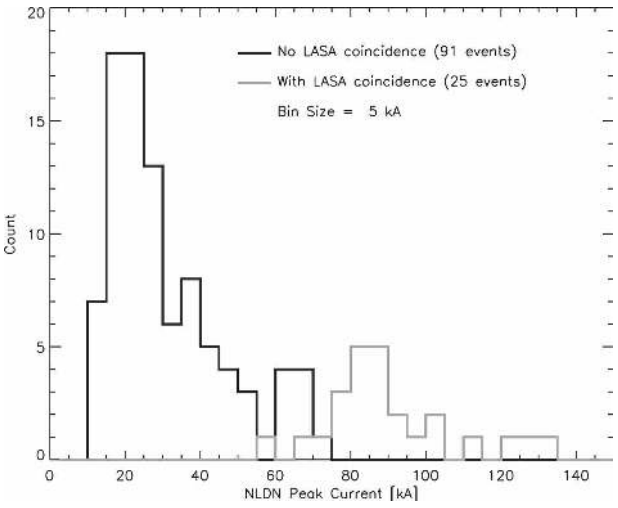

FIG. A4. Histograms of the absolute value of NLDN peak current for the 116 NLDN events from 0000 to 0115 UTC within the 22 Jun 2000 storm under study. Black line shows the distribution for NLDN events with no LASA coincidence. Gray line shows the distribution for NLDN events with LASA coincidence.

the NBEs in the storm on 22 June. As shown in Table A1, the NLDN-reported peak currents of the NBEs were all above 60 kA, with a mean of 90 kA.

This NLDN misclassification issue seems to be exclusive to positive CG strokes in this storm, as none of the NLDN-reported negative CG strokes were identified as NBEs by the LASA. As shown by the histograms of NLDN peak current in Fig. A4, LASA detected only the strongest events. There were 71 NLDN-reported positive CG strokes in this storm that LASA did not detect. We cannot determine whether these were also NBEs, but the foregoing analysis casts suspicion on the NLDN classification of these events as well.

d. Implications for other STEPS storms

One of the main purposes of STEPS was to investigate storms that produced PPCG lightning. Identification of PPCG behavior relies on the NLDN data. If the NLDN was mistaking NBEs for positive CG strokes throughout the STEPS project, the implications are alarming. There are already several published studies of storms during STEPS. We have briefly investigated the LASA observations of two of these storms to assess whether conclusions based on the NLDN data need to be reevaluated. LASA did not detect any NBEs in the 19 June 2000 storm of this study. LASA did not detect any NBEs in the 29 June 2000 supercell storm studied by Tessendorf et al. (2005) and Wiens et al. (2005). Hence, to the extent that the LASA observations allow, the conclusions based on the NLDN reports in these studies are not directly challenged.

LASA did detect hundreds of NBEs in a mesoscale convective system (MCS) that was situated just northeast of the supercell on 29 June 2000. NLDN reported hundreds of positive CG strokes in this MCS. Further analysis of the NBE and positive CG reports in this MCS (and other STEPS storms) is clearly warranted, but is beyond the scope of this study.

REFERENCES

Carey, L. D., and S. A. Rutledge, 1998: Electrical and multiparameter radar observations of a severe hailstorm. *J. Geophys. Res.,* **103,** 13 979–14 000.

——, and ——, 2003: Characteristics of cloud-to-ground lightning in severe and nonsevere storms over the central United States from 1989–1998. *J. Geophys. Res.,* **108,** 4483, doi:10.1029/2002JD002951.

Coleman, L. M., T. C. Marshall, M. Stolzenburg, T. Hamlin, P. R. Krehbiel, W. Rison, and R. J. Thomas, 2003: Effects of charge and electrostatic potential on lightning propagation. *J. Geophys. Res.,* **108,** 4298, doi:10.1029/2002JD002718.

Cummins, K. L., M. J. Murphy, E. A. Bardo, W. L. Hiscox, R. B. Pyle, and A. E. Pifer, 1998: A combined TOA/MDF technology upgrade of the U.S. National Lightning Detection Network. *J. Geophys. Res.,* **103** (D8), 9035–9044.

Grumm, R. H., J. D. Ross, and P. G. Knight, 2005: Examining severe weather events using reanalysis datasets. Preprints, *21st Conf. on Weather Analysis and Forecasting/17th Conf. on Numerical Weather Prediction,* Washington, DC, Amer. Meteor. Soc., CD-ROM, P1.87.

Kasemir, H. W., 1960: A contribution to the electrostatic theory of lightning discharge. *J. Geophys. Res.,* **65,** 1873–1878.

Krehbiel, P. R., R. J. Thomas, W. Rison, T. Hamlin, J. Harlin, M. Stanley, J. Lombardo, and D. Shown, 2000a: Inverted polarity lightning in STEPS. *Eos, Trans. Amer. Geophys. Union,* **81** (Suppl.), Abstract A62D06.

——, ——, ——, ——, ——, and M. Davis, 2000b: GPS-based mapping system reveals lightning inside storms. *Eos, Trans. Amer. Geophys. Union,* **81,** 21–25.

Kuhlman, K. M., C. L. Ziegler, E. R. Mansell, D. R. MacGorman, and J. M. Straka, 2006: Numerical simulations of the 29 June 2000 STEPS supercell: Microphysics, electrification, and lightning. *Mon. Wea. Rev.,* **134,** 2734–2757.

Lang, T. J., and S. A. Rutledge, 2002: Relationships between convective storm kinematics, precipitation, and lightning. *Mon. Wea. Rev.,* **130,** 2492–2506.

——, and Coauthors, 2004: The Severe Thunderstorm Electrification and Precipitation Study. *Bull. Amer. Meteor. Soc.,* **85,** 1107–1125.

Le Vine, D. M., 1980: Sources of the strongest RF radiation from lightning. *J. Geophys. Res.,* **85,** 4091–4095.

Liu, H., and V. Chandrasekar, 2000: Classification of hydrometeors based on polarimetric radar measurements: Development of fuzzy logic and neuro-fuzzy systems and in situ verification. *J. Atmos. Oceanic Technol.,* **17,** 140–164.

MacGorman, D., and Coauthors, 2002: Lightning relative to precipitation and tornadoes in a supercell storm during MEaPRS. Preprints, *21st Conf. on Severe Local Storms,* San Antonio, TX, Amer. Meteor. Soc., 423–426.

——, W. D. Rust, P. Krehbiel, E. Bruning, and K. Wiens, 2005: The electrical structure of two supercell storms during STEPS. *Mon. Wea. Rev.,* **133,** 2583–2607.

Mansell, E. R., D. R. MacGorman, C. Ziegler, and J. M. Straka, 2002: Simulated three-dimensional branched lightning in a numerical thunderstorm model. *J. Geophys. Res.,* **107,** 4075, doi:10.1029/2000JD000244.

——, ——, C. L. Ziegler, and J. M. Straka, 2005: Charge structure and lightning sensitivity in a simulated multicell thunderstorm. *J. Geophys. Res.,* **110,** D12101, doi:10.1029/2004JD005287.

Marshall, T. C., and M. Stolzenburg, 2002: Electrical energy constraints on lightning. *J. Geophys. Res.,* **107,** 4052, doi:10.1029/2000JD000024.

——, D. W. Rust, and M. Stolzenburg, 1995: Electrical structure and updraft speeds in thunderstorms over the southern Great Plains. *J. Geophys. Res.,* **100,** 1001–1015.

Mazur, V., 2002: Physical processes during development of lightning flashes. *C. R. Phys.,* **3,** 1393–1409.

——, and L. H. Ruhnke, 1993: Common physical processes in natural and artificially triggered lightning. *J. Geophys. Res.,* **98,** 12 913–12 930.

Mohr, C. C., and R. L. Vaughn, 1979: An economical approach for Cartesian interpolation and display of reflectivity factor data in three-dimensional space. *J. Appl. Meteor.,* **18,** 661–670.

——, L. J. Miller, R. L. Vaughn, and H. W. Frank, 1986: On the merger of mesoscale data sets into a common Cartesian format for efficient and systematic analysis. *J. Atmos. Oceanic Technol.,* **3,** 143–161.

Nelson, S. P., 1987: The hybrid multicellular-supercellular storm—An efficient hail producer. Part II: General characteristics and implications for hail growth. *J. Atmos. Sci.,* **44,** 2060–2073.

O'Brien, J. J., 1970: Alternative solutions to the classical vertical velocity problem. *J. Appl. Meteor.,* **9,** 197–203.

Perez, A. H., L. J. Wicker, and R. E. Orville, 1997: Characteristics of cloud-to-ground lightning associated with violent tornadoes. *Wea. Forecasting,* **12,** 428–437.

Rison, W., R. J. Thomas, P. R. Krehbiel, T. Hamlin, and J. Harlin, 1999: A GPS-based three-dimensional lightning mapping system: Initial observations in Central New Mexico. *Geophys. Res. Lett.,* **26,** 3573–3576.

Rust, W. D., and D. R. MacGorman, 2002: Possibly inverted-polarity electrical structures in thunderstorms during STEPS. *Geophys. Res. Lett.,* **29,** 1571, doi:10.1029/2001GL014303.

——, and Coauthors, 2005: Inverted-polarity electrical structures in thunderstorms in the Severe Thunderstorm Electrification and Precipitation Study (STEPS). *Atmos. Res.,* **76,** 247–271.

Saunders, C. P. R., and S. L. Peck, 1998: Laboratory studies of the influence of the rime accretion rate on charge transfer during graupel/crystal collisions. *J. Geophys. Res.,* **103,** 13 949–13 956.

——, W. D. Keith, and R. P. Mitzeva, 1991: The effect of liquid water on thunderstorm charging. *J. Geophys. Res.,* **96,** 11 007–11 017.

Smith, D. A., and Coauthors, 1999: A distinct class of isolated intracloud lightning discharges and their associated radio emissions. *J. Geophys. Res.,* **104,** 4189–4212.

——, K. B. Eack, J. Harlin, M. J. Heavner, A. R. Jacobson, R. S. Massey, X. M. Shao, and K. C. Wiens, 2002: The Los Alamos Sferic Array: A research tool for lightning investigations. *J. Geophys. Res.,* **107,** 4183, doi:10.1029/2001JD000502.

——, M. J. Heavner, A. R. Jacobson, X. M. Shao, R. S. Massey, R. J. Sheldon, and K. C. Wiens, 2004: A method for determining intracloud lightning and ionospheric heights from VLF/LF electric field records. *Radio Sci.,* **39,** RS1010, doi:10.1029/2002RS002790.

Stolzenburg, M., W. D. Rust, and T. C. Marshall, 1998: Electrical structure in thunderstorm convective regions. 3. Synthesis. *J. Geophys. Res.,* **103,** 14 097–14 108.

Straka, J. M., D. S. Zrnic, and A. V. Ryzhkov, 2000: Bulk hydrometeor classification and quantification using polarimetric radar data: Synthesis of relations. *J. Appl. Meteor.,* **39,** 1341–1372.

Takahashi, T., 1978: Riming electrification as a charge generation mechanism in thunderstorms. *J. Atmos. Sci.,* **35,** 1536–1548.

Tessendorf, S. A., L. J. Miller, K. C. Wiens, and S. A. Rutledge, 2005: The 29 June 2000 supercell observed during STEPS. Part I: Kinematics and microphysics. *J. Atmos. Sci.,* **62,** 4127–4150.

——, K. C. Wiens, and S. A. Rutledge, 2007: Radar and lightning observations of the 3 June 2000 electrically inverted storm from STEPS. *Mon. Wea. Rev.,* **135,** 3665–3681.

Thomas, R., P. Krehbiel, W. Rison, J. Harlin, T. Hamlin, and N. Campbell, 2003: The LMA flash algorithm. *Proc. 12th Int. Conf. on Atmospheric Electricity,* Versailles, France, ICAE, 655–656.

——, ——, ——, S. J. Hunyady, W. P. Winn, T. Hamlin, and J. Harlin, 2004: Accuracy of the Lightning Mapping Array. *J. Geophys. Res.,* **109,** D14207, doi:10.1029/2004JD004549.

Wiens, K. C., 2005: Kinematic, microphysical, and electrical structure and evolution of thunderstorms during the Severe Thunderstorm Electrification and Precipitation Study (STEPS). Ph.D. thesis, Colorado State University, Fort Collins, CO, 295 pp.

——, S. A. Rutledge, and S. A. Tessendorf, 2005: The 29 June 2000 supercell observed during STEPS. Part II: Lightning and charge structure. *J. Atmos. Sci.,* **62,** 4151–4177.

Willet, J. C., J. C. Bailey, and E. P. Krider, 1989: A class of unusual lightning electric field waveforms with very strong high-frequency radiation. *J. Geophys. Res.,* **94,** 16 255–16 267.

Williams, E. R., 1989: The tripole structure of thunderstorms. *J. Geophys. Res.,* **94,** 13 151–13 167.

——, 2001: The electrification of severe storms. *Severe Convective Storms, Meteor. Monogr.*, No. 50, Amer. Meteor. Soc., 527–561.

——, M. E. Weber, and R. E. Orville, 1989: The relationship between lightning type and convective state of thunderclouds. *J. Geophys. Res.,* **94,** 213–220.

——, V. Mushtak, D. Rosenfeld, S. Goodman, and D. Boccippio, 2005: Thermodynamics conditions favorable to superlative thunderstorm updraft, mixed phase microphysics and lightning flash rate. *Atmos. Res.,* **76,** 288–306.